A HOLISTIC CONTRIBUTION TO FAST INNOVATION IN ELECTRIC VEHICLES: AN OVERVIEW OF THE DEMOBASE RESEARCH PROJECT

A. Bordes[1], D.L. Danilov[2], P. Desprez[*3], A. Lecocq[1], G. Marlair[1], B. Truchot[1], M. Dahmani[3], C.Siret[3], S.Laurent[3], S. Herreyre[3], A. Dominget[3], L. Hamelin[3], G. Rigobert[3], S. Benjamin[3], N. Legrand[3], M. Belerrajoul[3], W. Maurer[4], Z. Chen[2], L.H.J. Raijmakers[2], D. Li[2], J. Zhou[2], P.H.L. Notten[2], P. Perlo[5], M. Biasiotto[5], R. Introzzi[5], M.Petit[6], J. Martin[6], J. Bernard[6], S. Koffel[7], V. Lonrentz[7], E. Durling[8], S. Korali[8], Z. Wang[9], M. Massazza[10], J. Lamontanara[10]

[1] Ineris, French National Institute For Industrial Environment And Risks, Parc technologique Alata BP 2, 60550 Verneuil-en-Halatte- France

[2] IEK-9, Forschungszentrum Jülich, D-52425 Jülich, Germany

[3] Saft, 111 bvd Alfred Daney, 33074 Bordeaux, France

[4] Infineon, Am Campeon 1-12 85579 Neubiberg, Germany

[5] IFEVS, carignano, 50/1 – 10040 La Loggia (To), Italy

[6] IFPEN, Rond-Point de l'échangeur de Solaize, 69360 Solaize, Farnce

[7] Fraunhofer Institut für Integrierte Système und Bauelementetechnologie, Schottkystrasse 10, 91058 Erlangen, Germany

[8] Modelon, Ideon Science Park, Beta 6 -SE-223 70 Lund, Sweden

[9] Accurec, Battaverstrasse 22 - 47870 Krefefd, Germany

[10] Ma, via Pavia 65, Rivoli (To) 10098, Italy

* Corresponding author: Philippe.desprez@acc-emotion.com

https://www.demobase-project.eu/

Abstract:

This paper is a contribution to fasten integration of battery pack innovation in commercial Electric Vehicles (EV) through massive digitalization: a seamless process detailed for battery design, battery safety, and battery management. Selected results of studies carried out on the EV value chain from design to recycling steps are presented, highlighting the importance of seamless integration and holistic state of mind when designing EV. Association between experimental and numerical approaches for efficient innovative EV production is crucial to achieve easy commercialisation. Successful forecasting of aging and thermal runaway evolution from single cell failure at module level using such methods illustrates their great potential. Hardware key counterparts under development are also introduced and give an idea of future architecture of EV battery packs and overall improvement of EV energy efficiency. Finally, a flexible and easily modifiable solution for battery electric vehicle (BEV) that allows rapid and cost-effective

1

40   integration of future innovation is presented. This paper globally illustrates key breakthroughs
41   gained in the context of the collaborative research project named 'DEMOBASE', for *DEsign and*
42   *MOdelling for improved BAttery Safety and Efficiency* successfully submitted for funding by the
43   European Commission in response to a 2017 call dedicated to 'Green Vehicles' under the EU
44   Horizon 2020 work programme "*Smart, green and integrated transport*".
45

46   Introduction:
47   The carriage electrification for personal transport began as early as in the 19th century. Prototypes
48   were built from the 1830s [1]. The first historical breakthrough towards electric vehicle development
49   was the invention of a new rechargeable battery technology, lead-acid batteries, by Gaston Planté's in
50   1859. Gustave Trouvé's tricycle in 1881 is nowadays recognized as the first electric vehicle [2].
51   However, the workability of this vehicle was very limited due to the existing electric power grid and
52   power supply system at that time. Then, continuous improvement led to an electric vehicle market
53   share weighing up to one-third of total vehicle sales in the early 1900s[1]. Vehicle electrification also
54   impacted the first racing cars with the famous rocket type electric vehicle nicknamed « *La Jamais*
55   *Contente* », which established a speed record at 105 km/h in 1899. However, the first successful
56   emergence of Electrical mobility was rapidly challenged by the vapor machine and eventually killed for
57   decades by the emergence of the internal combustion engine (ICE).

58   In the early 20th century, the internal combustion engine took advantage of all other automobile
59   propulsion modes. It was pushed by widely spread and low-cost oil, among other technical benefits,
60   including mileage capacity. In fact, a lead-acid battery has a specific energy of 30 Wh/kg when diesel
61   fuel combustion generates around 13 000 Wh/kg of energy. So, even considering 30% efficiency for
62   the propulsion and the need to integrate a gasoline tank in the vehicle, the system proved to be the
63   most efficient for cars. Apart from the technical advantages of ICE-fired cars over electric vehicles, the
64   emerging market price of ICE cars was the second killer of first electric car fleets in the US: the famous
65   Ford T model was sold some 650 US $ by 1912 while an electric roadster was costing around 1750 US
66    $ at the same time[3].

67   While some revival in the early 1990s of lead-acid and Ni/Cd electric cars appeared, by the end of the
68   20th century, two root causes have initiated a vehicle paradigm change. On the one hand, a new
69   regulation was enforced by the law requiring a sharp reduction of major pollutants in vehicles' exhaust
70   gases. On the other end, Li-ion technology innovation was introduced on the market with the first
71   product made commercially by Sony in 1991. In the 21st century, the late awareness of fast emerging
72   environmental concerns, the recognition that existing fossil resources are limited, and ultimately the
73   significant impact of some international conferences on climate change led to establishing regulations
74   setting new restrictions for the use of thermal vehicles. Power Metal Oxide Semiconductor Field Effect
75   Transistor (MOSFET) invention in 1970 also sharply improved energy efficiency in an electric vehicle.
76   In the 2009 EU roadmap, it has been demonstrated that a mid-size electric car could lead to primary
77   energy saving of 30%[4]. At the origin of electric vehicle revival, Lithium-ion (Li-ion) technology
78   provides two key advantages the desirable high energy density achieved thanks to aprotic electrolyte,
79   and extensive cycling capability achieved thanks to Li insertion process in layered host structures. The
80   benefit of aprotic electrolyte providing a larger electrochemical operating window for the lithium-ion
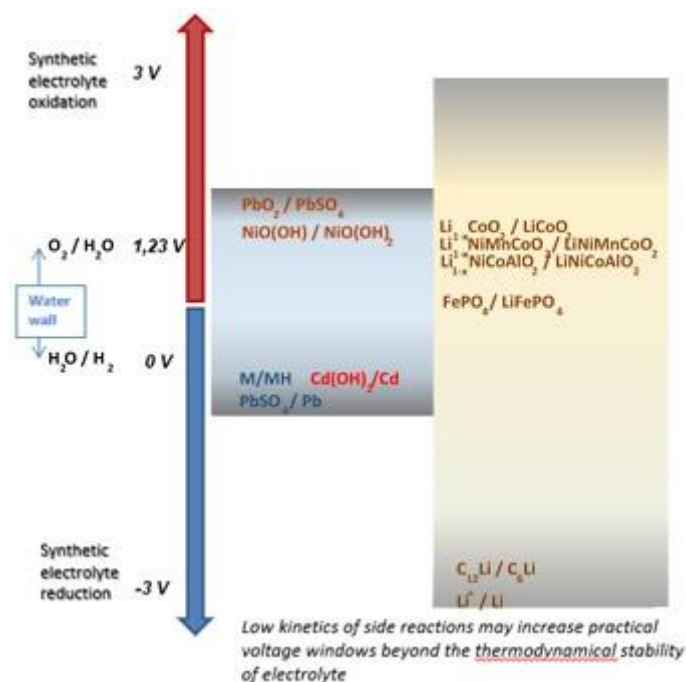81   battery over the lead acid system is illustrated in **Figure 1.**

Figure 1: Overview of different battery systems with aqueous and aprotic electrolytes.

The technical innovation was supported by large investment. Between 2009 and 2015, about 10 to 12 billion dollars were invested worldwide in lithium-ion battery production. The investment was favoured by public funding, like the American Recovery and Reinvestment Act of 2009. In Europe, The European Battery Alliance (EBA) was launched in October 2017 by Vice President Šefčovič who reported that "*Batteries are at the heart of the industrial revolution and I am convinced that Europe has what it takes to become the world's leader in innovation, decarbonization, and digitization*"[5].

Consequently, lithium-ion costs through Giga-factory production and associated supply chains sharply decreased. The global electric car fleet was counting some 5 million units in 2018[6].

The automotive pack cost is in constant diminution and is today approaching 100$/kWh for NMC high energy density cells [7-10]. Consequently, cost parity amongst ICE and EVs becomes closer and closer. In fact, low speed EVs are currently sold in China at a price ranging from less than 4000 euros with a battery pack of 9.3 kWh to 10500 euros with battery packs of 31.9 kWh [11]. The total Cost of Ownership (TCO) of EVs is already lower than the ICE counterparts [12] and the expectation is that the production cost of EVs will also decrease very soon [13]. Emerging technologies and drastic cost reductions are changing the landscape of urban mobility leading to new business models including semi-autonomous and fully autonomous electric vehicles for the mobility of people and goods [14].

Indeed by 2030, most of the world's population will be concentrated in cities. Assuming today's trend continues, by 2050, more than 80% of the world's population will live in an urban environment. Cities are places of innovation; they are the drivers of our economy and areas where wealth and jobs are created. That is an opportunity for light electric vehicles and buses, illustrated by their fast growth in the urban mobility industry. The electric vehicle all together leads to a mind shift in mobility and energy use [14]. In this quickly evolving market targeting ambitious innovations related is crucial. In this respect the DEMOBASE EU research project has considered the most critical aspects: Safety, Robustness over time, Fail operational and fail aware battery management (24*7 service capability), high performance in all climates, ergonomics, affordability through low-investment manufacturing at vehicle level, new power electronics, and recyclability.

111 The first concern is battery degradation and performance over time. Electric-car batteries lose capacity
112 over time—though not nearly as fast as those for consumer-electronics devices with a 1- to 4-year
113 expected life. Losing 10 percent of capacity over an 8- or 10-year warranty is not too big a deal, but
114 losing 40 percent would be.

115 The second short term concern is the vehicle production cost. It is mainly related to the battery cost,
116 representing today around 30%-40% (see 2013 cost information in [15]) of the complete vehicle price.
117 The price includes direct production costs and upfront investment to start manufacturing a new
118 vehicle.

119 Today fail-safe concept stops battery operation when one cell is outside safe conditions. While
120 DEMOBASE battery system using a fail-operational concept and fail aware battery management could
121 maintain the battery and the car operational. Fail aware functions provide the battery safety state of
122 the vehicle in operation to forbid vehicle use in restricted areas, like channels, and to the faster
123 maintenance operation.

124 To achieve these challenging goals, the DEMOBASE concept relies on massive digitalization together
125 with a seamless process integrating battery design, battery safety, and battery management.

126 After demonstrating the interest of a software collaborative platform on a multi stakeholder
127 environment, the research has promoted the combination of both experimental and numerical studies
128 in particular to forecast aging and safety parameters at module level. To tackle safety issues that are
129 crucial, the modules were designed with a fail-safe approach. A full-scale test was conducted to
130 validate model predictions and to measure emissions (fumes and particles) in case of field failure of
131 battery pack modular components. In addition to the fail-safe design concept, an innovative Battery
132 Management System (BMS) using neural network for its operation was investigated to estimate
133 battery state parameters and to track early stage default.

134 Hardware key counterparts under development is also introduced and give an idea of future
135 architecture of EV battery packs and overall improvement of EV energy efficiency. Eventually a flexible
136 and easily modifiable solution for battery electric vehicle (BEV) that allows fast integration of future
137 innovation at a low investment cost production is presented. In this study, the dismantling and
138 recycling stages were included as they are a core part of sustainable EV design, even if yes too often
139 considered as minor aspects or just ignored at design stage of an EV.

140 Subsequently and globally, this article aims at briefly presenting key results of studies carried out on
141 the EV value chain from design to recycling in order to highlight the though process of a holistic and
142 fast EV development process. More details in the scientific underpinning approaches developed in the
143 DEMOBASE project and major breakthrough achieved have been made available as separate
144 communications or dedicated publications. Relating information in the matter, as well as on the
145 organization of the DEMOBASE project itself has been made available to the readers in supplementary
146 information.

147   1.   Vehicle Design and seamless digital process
148   1.1. Proposition for a software (SW) collaborative platform
149 A collaborative platform for integrating simulation models has been developed and demonstrated
150 within the project. The platform is a proof-of-concept that demonstrates how to achieve a common
151 integration and system simulation toolchain, within a project of several partners that create sub-
152 systems models in different software tools.

153 The platform is based on the open FMI (Functional Mock-up Interface) [16] which has become the de-
154 facto standard for exchanging simulation models between different softwares within the automotive
155 industry. With this standard, dynamics models are exported and exchanged as FMUs (Functional Mock-
156 up Units).

157 The platform allows integrating several sub-system FMUs into a single system FMU, that can be
158 simulated directly within this toolchain or imported into any simulation software that supports the FMI
159 standard. The platform employs the Python based Jupyter Notebook scripting environment for
160 interfacing and controlling the integration and simulation of the FMUs. This allows both interactive
161 and automated execution of the integration and simulation process. The simulation of the system FMU
162 is carried out through the open source PyFMI Python package (for simulation of FMUs via Python). The
163 FMU integration is carried out via a Python wrapper package for an external Java module (*the FMI
164 Composer backend*) that has been utilized and further developed within the project.

165 A case study was conducted for evaluating the platform in a relevant scenario. In this scenario, a
166 physics based electric powertrain model was exported as one FMU, which was combined with a
167 separate battery control software model exported as another FMU. The powertrain model was
168 implemented in the Modelica modeling language [17] using the Electrification Library and the Modelon
169 Impact software. The battery controller software model was implemented in Matlab/Simulink. A test
170 case was created for the system for simulating a charging procedure of the battery, to demonstrate
171 the interaction between the separate physics and controller of the battery in the powertrain system.
172 Part of the case study was to demonstrate how causal plant and controller model interfaces could be
173 set-up to allow integration with external model.

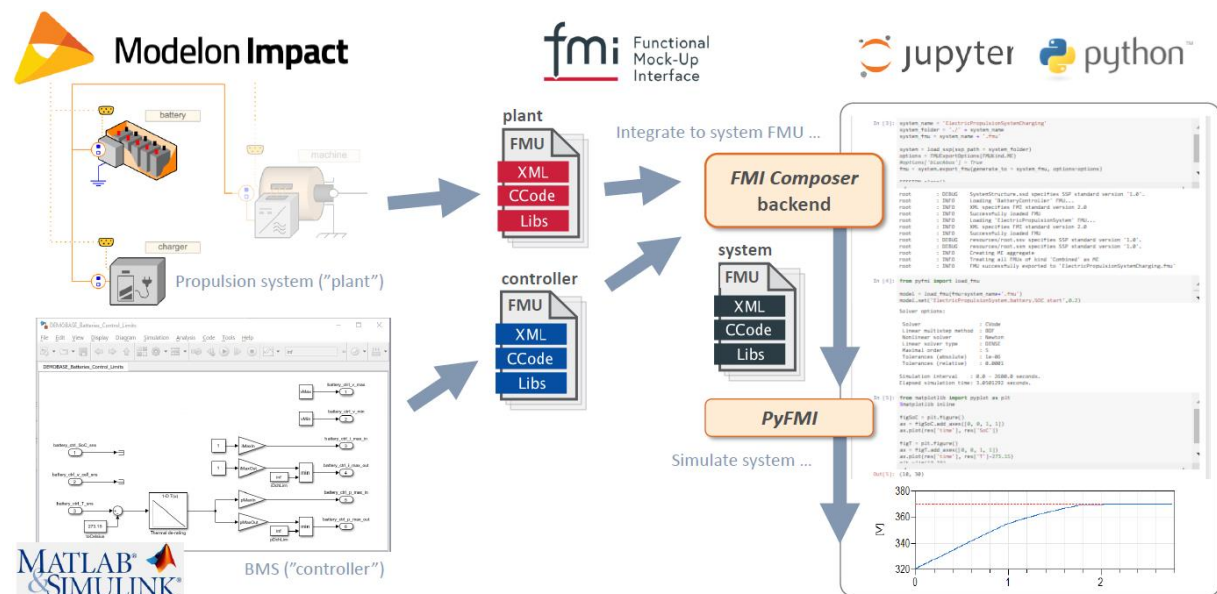174 The elements of the toolchain and integration/simulation platform is seen in Figure 2.

175
176

177 **Figure 2: Plant model FMU from Modelon Impact, and controller FMU from Simulink,**
178 **combined and simulated as a single system FMU.**

179

180 This platform has also served as a proof-of-concept for achieving democratization of simulation
181 models, where complex dynamic system models are made available to non-expert model users via a
182 web browser interface. This has been demonstrated for both a single Modelica modeling environment

5

(Modelon Impact), and for simulating models integrated from several tools via the Jupyter notbook interface.

Furthermore, it has also been demonstrated within the project how an automated integration and simulation procedure could be executed as part of a continuous integration (CI) toolchain, using the Jenkins software, and using this for regression testing to track changes to simulation results for a system of FMUs.

1.2. Cell design and testing tools and methods
Guiding principles for cell design was developed in order to facilitate easy assembly of several generations of cells, as well as easy and scalable safety testing

1.2.1. Cells with heater for safety tests

The prototyping from cells to vehicle has been enabled by the development of original equipment. Pouch cells will be stacked in module or directly in the vehicle battery pack or chassis.

Whatever its implementation, mechanical integration can influence cell performance longevity. Specific holders have been developed for this purpose to mimic genuine cell constraints inside a module. The Figure 3 presents a cell holder developed to set cell pressure during electrical tests. This sample holder was also used for aging studies (see sections 1.2.2 and 1.2.3).
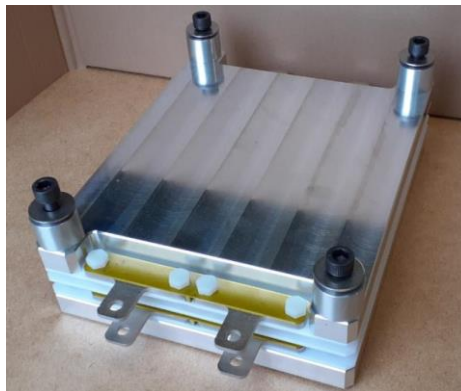

Figure 3: Cell Holder to mimic module environment.

It is well-known that cell internal short-circuit has a very low probability of occurrence due to manufacturing defects (below 10 ppm for consumer cells, down to ~ 0.05 ppm for screened commercial cells for spacecraft application [18]). However internal short in a cell remains an event that has to be considered for the system global safety. The internal short circuit root cause can come from pollution at production level or wrong cell integration in the final product for example.

To assess this safety issue at very early development stage, a specific pouch cell has been developed with an embedded internal heater. The heater power is managed by an external power supply. Figure 4 presents the specific pouch cell with two terminals on its side to power the internal heater.
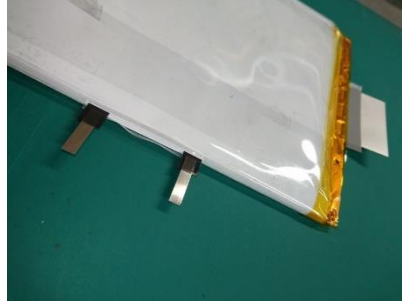
214

Figure 4: Pouch cell with internal heater.

216

Testing different chemistries at cell level, with high fidelity of the final cell constraint at battery level participates to fast introduction of battery innovation at BEV level. Moreover, pouch cell equipped with this internal heater as shown in Figure 4 has been successfully used to study short-circuit consequence at cell, cluster of cells and module levels and confirm fail-safe behaviour of the entire battery pack from this view point.

1.2.2. Methodology to assess cell aging

The degradation of the modern mass-produced Li-ion battery is a complex and versatile process. F Figure 5a) illustrates the main driving factors, degradation mechanisms, their interactions, and consequences. Red and blue arrows indicate processes happening with ($I \neq 0$) and without ($I = 0$) application of the current. Absence of current implies no volume change $\Delta Vol = 0$ and aging process is reduced to Solid Electrolyte Interface formation on the surface of anode particles. This surface denoted A^{cov}, because in such situations surface of the particles is covered by the SEI. Resulting loss of electrochemically active lithium imply decline of capacity denoted as ΔQ_{ir}. In general, the irreversible capacity loss depends on many factors, including metal deposition on anode and decay of anode material, denoted as ΔQ_{C_6}. Cathode material also can decay, dissolve, and corresponding capacity decline is denoted as ΔQ_c. The cycling induced aging is more complex process, arising from the volume changes during operation $\Delta Vol \neq 0$. This volume change leads to the opening of fresh uncovered surface on anode particles, which is denoted as A^{fr}. SEI formation on freshly opened surface is especially intense. More details about complex crosslink between various degradation factors can be found in Li *et al.* [19].
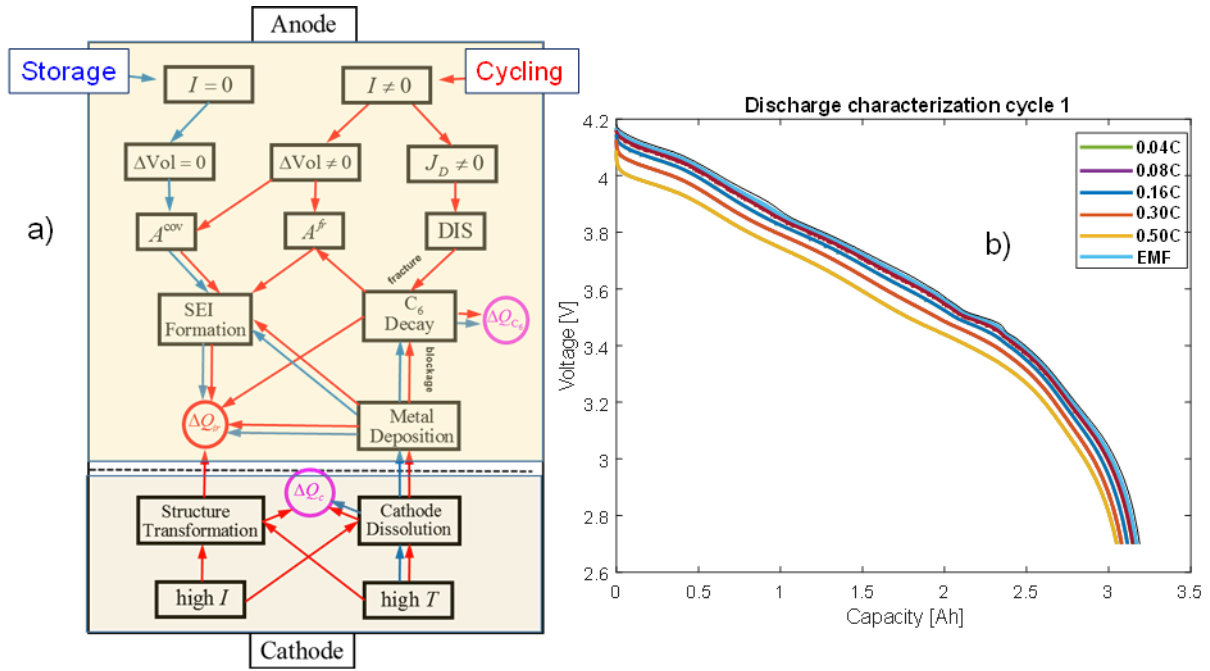
Figure 5: a) Complexity of aging processes in modern Li-ion batteries. b) Characterization of NCA cell: static discharge voltages and estimated EMF.

From the scheme, one can conclude that for an accurate description of the aging of Li-ion cells, at least three primary degradation mechanisms should be considered: the loss of electrochemically active lithium, the degradation of the positive electrode (cathode) active material, and the degradation of the negative electrode (anode) active material. As an object for the experiment, 3.2 Ah cylindrical cells with Nickel Cobalt Aluminium cathode and mixed graphite/Si/SiOx anode had been selected; cells were provided by TianJin Lishen Battery Joint-Stock CO., LTD. The aging experiment's main building brick is a regular and well-defined characterization sequence, repeated systematically during the aging experiment. Notation (T, Cch, Cdis) indicates cycling experiment performed under ambient temperature T, under Constant Current Constant Voltage (CCCV) charging protocol, with constant current C-rate Cch and constant current discharge C-rate Cdis. For example (25 °C, 0.3C, 1C) corresponds to a cycling experiment performed under an ambient temperature of 25 °C, charging with 0.3C and discharging with 1C rates. Cut-off current in the CV part was set to 120 mA in all experiments. All cycling experiments are organized in the following way. At the beginning of the investigation, the standard-characterization is applied. The standard characterization is a sequence CCCV charging (1 C in the CC part with the upper voltage threshold 4.2 V) and CC discharging with various C-rates until 2.8 V. Figure 5b) shows the characterization experiment performed at the ambient temperature of 25 °C. For electromotive force (EMF) estimation, extrapolation to the zero current was applied (as detailed in previous work [20]). The maximal capacity is defined at a charge extracted until EMF drops to 2.8 V.

The classic cycling experiment for a fixed cell consists of repeated CCCV charging and CC discharging, separated by a short rest period. Figure 6a) illustrates fade in the cell's extracted capacity when cycled with 0.3 CC charging and 1 C discharging current.
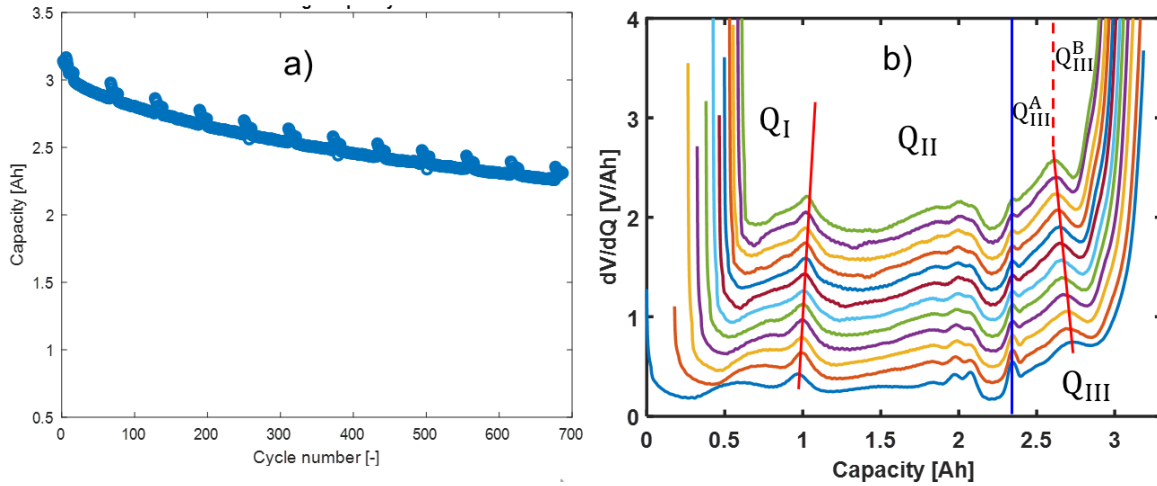
Figure 6: a) Capacity fade during (0.3C, 1C) cycling experiment. (b) Differential voltage analysis for the same experiment. The lowest line represents dV$_{EMF}$/dQ function for the fresh cell. Each next line in the vertical direction corresponds to dV$_{EMF}$/dQ obtained during the subsequent characterization

Figure 6b) shows differential equilibrium voltage analysis for the same cell, performed according to Lee *et al.* [21]. The lowest line represents dV$_{EMF}$/dQ function for the fresh cell. Each next line in the vertical direction corresponds to dV$_{EMF}$/dQ obtained during the next characterization. Characterization is performed approximately after a month of cycling. Analyzing cycling experiments with varying charging current (25 °C, 0.1C, 0.3C), (25 °C, 0.5C, 0.3C), (25 °C, 1C, 0.3C), (25 °C, 1.8C, 0.3C) it was also found that charging regime is profoundly important for aging. In particular, it was discovered that charging with high C-rates causes accelerated aging of the cells with short-circuiting (most likely due to lithium plating) after a few hundred cycles, see Figure 7a. In contrast, analyzing set of cycling experiments with varying discharging current (25 °C, 0.3C, 0.1C), (25 °C, 0.3C, 0.5C), (25 °C, 0.3C, 1C), (25 °C, 0.3C, 1.8C) it was concluded that discharging regimes have little influence on the aging (see Figure 7b). In all cases, the main degradation mechanism was lithium consumption, while the degradation of electrode materials was minor.
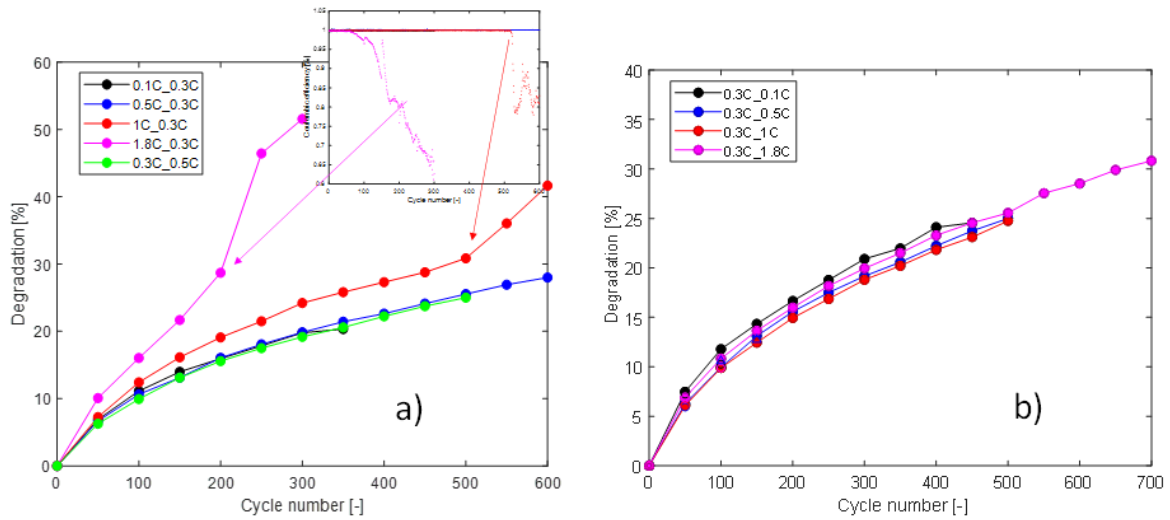
Figure 7: a) Influence of the charging regime on capacity degradation during cycling with the various charging current. The inset contains Coulombic efficiency for the two highest C-rates. b) Influence of discharging regime on capacity degradation.

1.2.3. Forecasting aging of advanced SiOx cells

One of the aims of the cycling experiments performed by Forschungszentrum Jülich in the DEMOBASE project was to find out if it is possible to predict the aging behavior of the cells with composite graphite Si/SiOx anode on the base of experiments with the calendar duration not more than 4 months. From cycling experiments, it follows that the main factor in the capacity loss of selected cells was lithium consumption. Therefore, the application of the lithium consumption model, according to Li *et al.* [22], is appropriate. Figure 8a) illustrates the aging model's performance for the case of (25°C, 0.3C, 0.1C) aging regime. Cells were cycled between V_{max} = 4.2 V and V_{min} = 2.7 V.
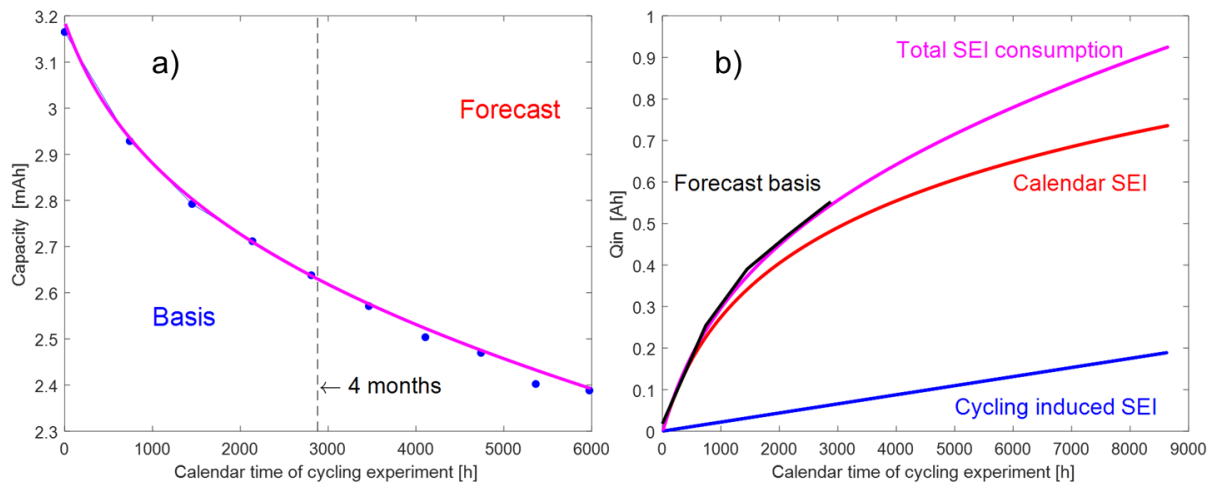

Figure 8: a) Aging forecast based on the 4-month experiment, blue dots are experimental data, and the pink line is the model prediction curve for comparison. b) Main components of the lithium consumption in the SEI layer.

305 It can be seen that, on the basis of 4 months of the experiment, the future aging of the battery can be
306 predicted pretty well; the last (8 months) point is deviating from the forecasted value less than one
307 percent. Figure 8b illustrates the main contributions of lithium consumption in the Solid Electrolyte
308 Interface (SEI). The pink line shows total lithium consumption in SEI, which also equals to capacity loss.
309 The red line shows lithium consumption on the stable part of the SEI, continuously growing according
310 to calendar time. The blue line corresponds to the freshly formed and subsequently peeled SEI, and,
311 therefore, is attributed to the cycling effect. The black line marks a basis for the forecast, the first 4
312 months of the experiment. It can be concluded that lithium consumption at the stable part of SEI is the
313 major contributing factor in battery capacity loss.

314

315 <u>1.3. EV performances design</u>
316 Cell performances need to be assessed in the scope of the complete vehicle system in order to take
317 into account all existing limitations such as current limits for battery usage as well as electric machine
318 and power electronic limitations. As a consequence, a complete EV simulator has been developed
319 based on IFEVS design using Simcenter Amesim™ software.

320 This simulator uses specific submodels from Simcenter Amesim libraries comprising Electrical Storage,
321 Drive libraries calibrated thanks to experimental data from IFPEN and IFEVS test benches. It has then
322 been validated against experimental data from the complete vehicle showing the accurate prediction
323 of vehicle energy consumption as well as maximum speed. Furthermore, it has been used in order to
324 provide the consortium a realistic power profile of the battery in use in the vehicle which can be used
325 in turn to validate and evaluate estimation or safety strategies.

326 In a second time, after validation, the vehicle simulator was integrated in a Hardware in the Loop (HiL)
327 system. In this experimental setup, whose synoptic view is shown in Figure 9, a single battery cell is
328 tested in a test bench with a climatic chamber with the whole vehicle system simulated on the control
329 computer. The link between modelling platforms and the experimental setup is ensured thanks to
330 xMOD software. This allows the fast assessment of a battery in a complete target system evaluating in
331 the same time the vehicle performance as well as the battery behaviour in realistic conditions. The HiL
332 system has been developed and tested using the first generation of DEMOBASE cells and then the
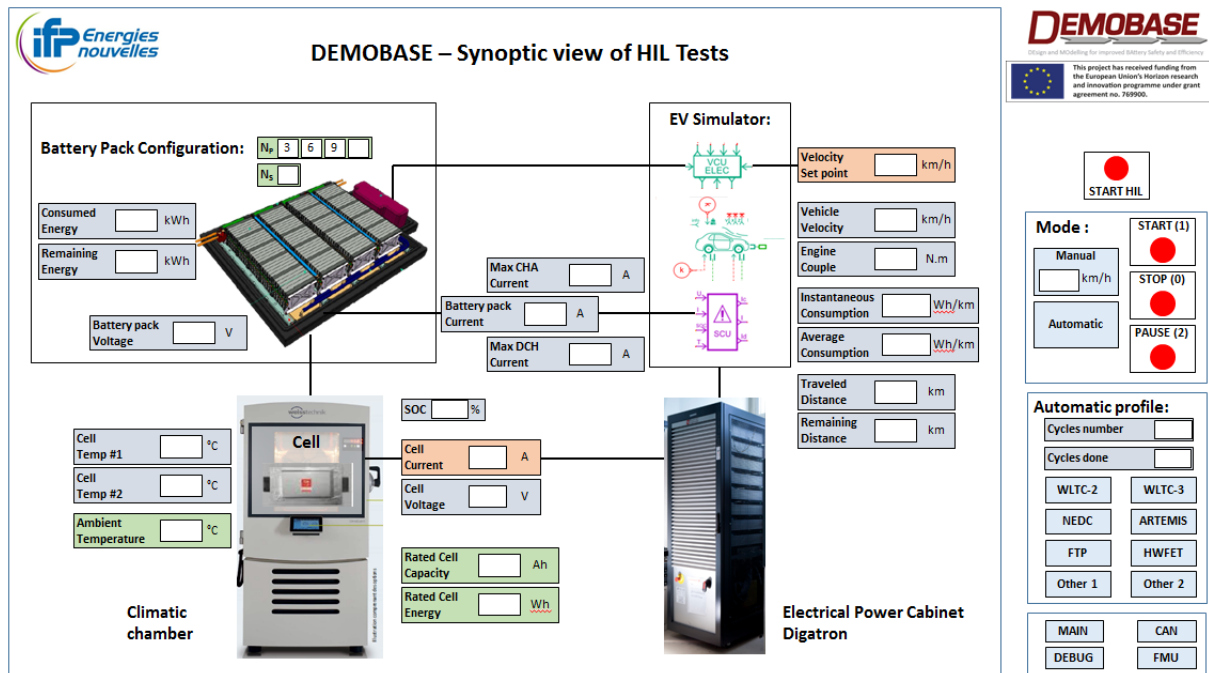333 second generation cell has been installed and assessed in the system.

334

Figure 9: Synoptic view of HiL tests.

Several parameters are adjustable by users concerning:

- The cell: users can adjust the cell specifications such as current or temperature limits, the initial state of charge, and the operating temperature.
- The pack: number of cells in series and number of parallel branches (see in the next paragraph, detailed information on battery pack architecture)
- The vehicle: the mission profile (WLTC, NEDC, Artemis…)

Some results are indicated in Table 1 where 4 duty cycles were tested, the influence of temperature and of the number of parallel branches has been assessed on a Worldwide Harmonized Light Vehicles Test Cycles (WLTC) 3.1 duty cycle. In order to assess the range of the vehicle, the tests are launched with the cell fully charged and duty cycles are repeated (iterations) until battery depletion occurring when the minimum voltage is reached.

The HiL system has been used on the 2 cells of the DEMOBASE project. As the performance of the 2nd generation of cells is highly increased compared to the first generation, as well as cell design, the pack design has been adjusted from 28s12p or 28s 9p for the first generation to 28s4p or 28s3p in the second generation. Besides the specific range (being the range of the vehicle divided by the mass of cells) is used to compare the performance of the battery system.

First regarding the duty profile, it shows that energy consumption of the duty profile comprising few high speed phases (urban ARTEMIS) is lower compared to high way duty cycles (HWFET) leading to higher urban range 193 km for 1st gen cells and 147 km for 2nd gen cells compared to 154 km and 120 km respectively.

In terms of comparison of the two generations of cells, at the level of average energy consumption, it appears at first glance that there is no difference between the two generations of cells, except for

362 slight differences in consumption for the tests WLTC / 1 branch / 25 ° C, WLTC / 3 branches / 5 ° C, and
363 NEDC / 3 branches / 25 ° C.

364 **Table 1: Impact of road profiles and cell on vehicle behaviour**

1st generation cell (HIL results)							
Road profile	Temp. (°C)	Branches	Active cells mass kg	Iterations	Range km	Specific range km/kg	Energy consumption Wh/km
WLTC 3.1	25 °C	4	162.96	16	248	1.52	87.8
WLTC 3.1	25 °C	3	122.22	12	188	1.54	87.7
WLTC 3.1	25 °C	2	81.48	8	122	1.49	87.9
WLTC 3.1	25 °C	1	40.74	4	57	1.39	89.7
WLTC 3.1	5 °C	3	122.22	11	172	1.40	88.0
NECC	25 °C	3	122.22	15	171	1.40	94.2
HWFET	25 °C	3	122.22	9	154	1.26	105.1
Urban Armetis	25 °C	3	122.22	39	193	1.58	84.3
2nd generation cell (Amesim simulation results, HIL test in progress)							
WLTC 3.1	25 °C	4	89.6	12	194	2.16	88.4
WLTC 3.1	25 °C	3	67.2	9	144	2.14	88.2
WLTC 3.1	25 °C	2	44.8	6	94	2.09	88.9
WLTC 3.1	25 °C	1	22.4	3	43	1.91	93.5
WLTC 3.1	5 °C	3	67.2	8	131	1.96	90.6
NEDC	25 °C	3	67.2	11	131	1.95	95.6
HWFET	25 °C	3	67.2	7	120	1.78	105.3
Urban Armetis	25 °C	3	67.2	29	147	2.18	86.7

365

366 But in fact, these slight deviations reflect significant differences in the behaviour of the packs
367 corresponding to these two generations of cells. The 1st generation cells, by their own characteristics
368 and the fact of being assembled by three (3p), lead to limit currents in charge and in discharge much
369 higher than with the 2nd generation cells. As a result, all speed profiles pass without problem with 1st
370 generation cells, which is not the case with 2nd generation cells: the discharge current limit is reached
371 for high speeds for the test WLTC / 1 branch / 25 ° C, and for the test NEDC / 3 branches / 25 ° C; the
372 charge current limit (in braking regeneration) has been reached for the test WLTC / 3 branch / 5 ° C.

373 Coming back to the 1st generation cells and the WLTC cycles, there is no limitation related to the
374 number of branches, and the autonomy is proportional to the number of cells in the pack. The
375 temperature has only a very weak effect in reducing the number of iterations by the premature
376 reaching of the low voltage limit of the cells.

377 Finally, both technologies can be compared one to another, for certain cycles, keeping in mind that
378 the total energy of both battery packs with the same number of parallel branches are different.
379 Consequently, the range using WLTC with 4 branches is higher with first generation (248 km compared
380 to 194 km) since the total amount of energy is higher in the 1st generation pack. However, the specific
381 range is higher in the 2nd generation pack (2.16 km/kg instead of 1.52 km/kg) emphasizing the better
382 performance of the 2nd generation cells, as long as the current limits are not reached.

383 Thanks to the HiL tests, not only fast assessment of the vehicle behaviour has been allowed for a given
384 cell to analyse the impacts of duty cycles and operating conditions but also a fast assessment of new
385 cell behaviour and its impact on the whole vehicle performances was also allowed.

386

387   1.4. Battery safety

388 Battery safety should be thought during early development phase of the battery pack and consider the
389 whole value chain, including recycling and possible development of emerging uses of EV like vehicle to
390 grid (V2G) in connection to the development of smart grids. In addition, the European directive on
391 vehicle end-of-life and European battery directive give in the field tights requirements on the battery
392 end-of-life.

393 When designing an EV, it seems important to take into account the last elements of the accidental
394 database and anticipate the evolution of the normative and regulation frame. It requires the active
395 participation or a follow-up of the different relevant working groups.

396

397   1.4.1. Battery pack architecture

398 The battery pack is design to allow fail operational function with a parallel branch configuration. The
399 number of branches defines cars portfolio according to their range. All cells are not connected in series,
400 which allow vehicle to be in operation even when losing a battery branch. Figure 10 describes the
401 battery pack architecture with 3 branches in parallel.

402
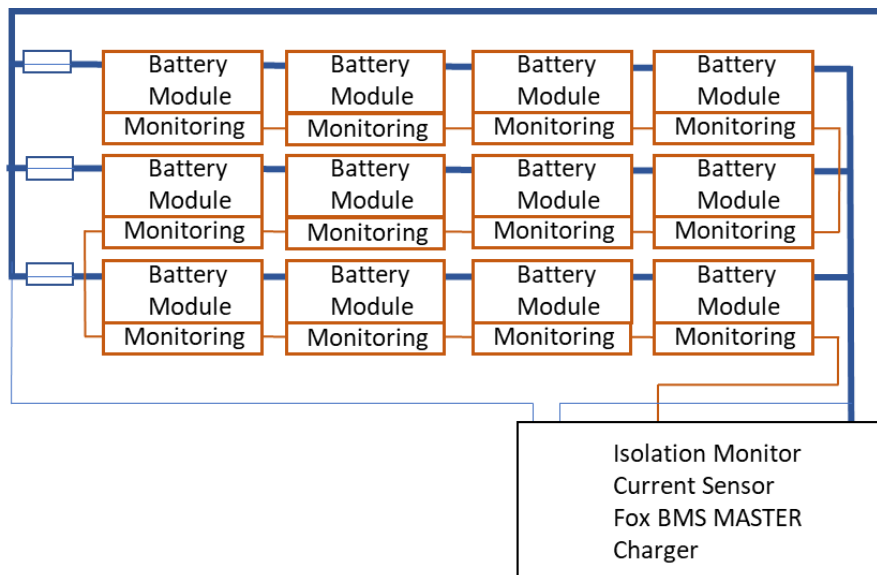
403 **Figure 10: DEMOBASE battery pack architecture.**

404

405   1.4.2. Gas flammability and emission toxicity

406 As a consequence of a battery thermal runaway event, a broad range of hazards can be produced:
407 electrical, chemical, thermal. Among this variety of hazards, gas emission is probably the most difficult
408 to evaluate but is paramount to ensure EV safety. Emitted gases are not only potentially toxic but can
409 also be flammable [23].

410 The properties of emitted gases are important as required inputs in risk assessment (underground
411 parking lots, vehicle passenger compartment, environmental considerations).

412 The nature, the volume and the way gases are emitted should be taken into account during the battery
413 pack design to implement a good gas management system.

414 In the DEMOBASE project, a gas analysis was performed during the validation test at module level
415 presented above. The module is composed of 9 NMC(111)/graphite flat pouch cells with a nominal

416 energy of 70 Wh each and a specific energy of 145 Wh/kg. Among the 9 cells composing the module,
417 thanks to the fail-safe architecture of the module, only 3 participated to the reaction and no flames
418 where observed during the thermal event. Main results of gas analysis are presented in Figure 11.
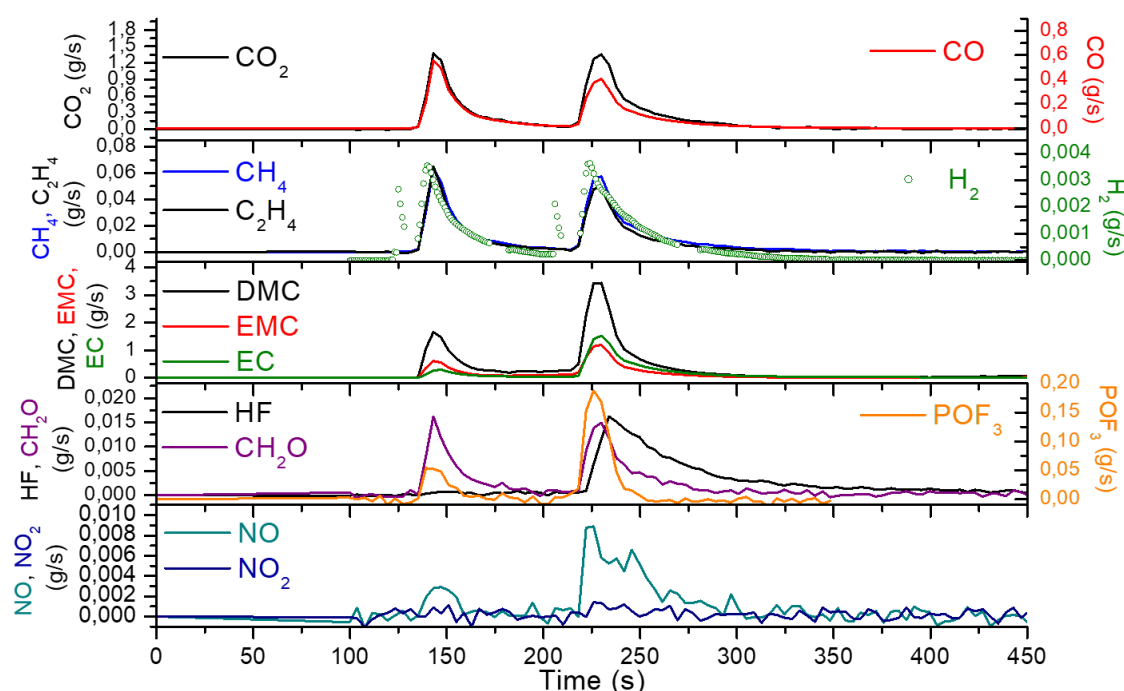

419
420

Figure 11: Main results of the gas analysis performed during the module short-circuit test.

422
423 The gas mixture is classical for a battery thermal runaway not resulting in flaming combustion. The
424 mostly emitted gases/vapors (in mass) are carbonates coming from the electrolyte. Lower quantities
425 of H_2 are also emitted but representing a consequent volume. Those gases are flammable and might
426 create an explosive atmosphere. On the toxic side HF emission and POF_3 are detected. These emissions
427 have to be taken into account to protect passengers or first responders in case of accident.

428 The study of emissions should not be limited to gases, particles should also be considered. That is why
429 in DEMOBASE project a metallic particle analysis using quartz and cellulosic filters was put in place.
430 Mains results are presented in Figure 12. More than 70% of particles mass came from the cathode
431 (NMC), 20% come from the lithium salt ($LiPF_6$) and 8% from positive current collector (Al). Probably
432 because of copper high melting point (1085°C), and since the module reacted without flaming
433 combustion process and as a consequence reached relatively low temperatures (425°C measured on
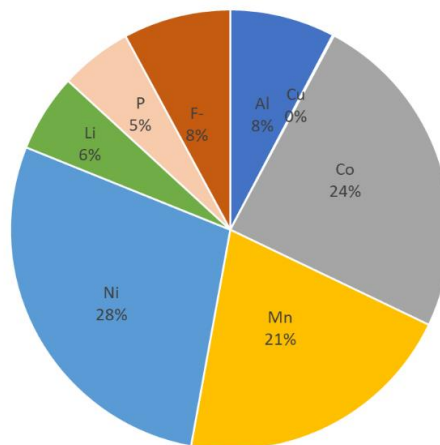434 the outside of the cell), no copper particle was detected.

435

Figure 12: main results of the particle analysis performed during the module short-circuit test.

The study of flammability and gas emission should not be limited at cell level and component level., Cell integration in a pack and pack integration to a vehicle can indeed add new gas components. In that context, plastic component selection for use in the battery pack developed in the DEMOBASE project was also studied in terms of fire safety aspects by fire calorimetry

One other input of the Computational Fluid Dynamic (CFD) model proposed is its capability to evaluate the combustion process and to predict the characteristics of emitted gases, based on experiments at cell scale. Using this smoke composition, toxic risk for the surrounding environment can then be estimated taking into account the dispersion process, typically solved by the fluid mechanic code.

1.4.3. Thermal runaway (TR) propagation

When the EV industry moved away from aqueous battery technologies to organic electrolytes, the hazardous profile of the batteries has drastically changed and the EV market face now the well-known thermal runaway hazard [24]. For years, research to find additives or compounds that prevent TR were conducted but the available feedback showed that the thermal runaway of one element in a battery pack cannot be ruled out for any battery technology or cell design. That is why safety feature of an EV should consider the limitation of the propagation of a TR from an element to another [25]. The battery industry and normative frame seems to be in agreement with this trend.

In the DEMOBASE project, a "fail-safe" approach has been chosen.

In this context, and to consider different phenomenon, several complementary models have been developed under different software platforms. All the models use experimental data as inputs or for model validation.

<u>1D thermal runaway propagation</u>

A detailed 1D thermo-chemical model of battery module thermal runaway has been developed by IFPEN using Simcenter Amesim. This model aims at fast computing simulation of thermal runaway propagation regarding several operating conditions, design and initiations [26]. Each element of the module (battery cell, compression pad, heat sink, bus bars, firewall etc.) is described as an 1D

submodel with lumped parameters as can be seen in Figure 13. For simplification sake, the module has been modelled as a 3p3s submodule.

a) 3P7S module structure proposed by I-FEVS
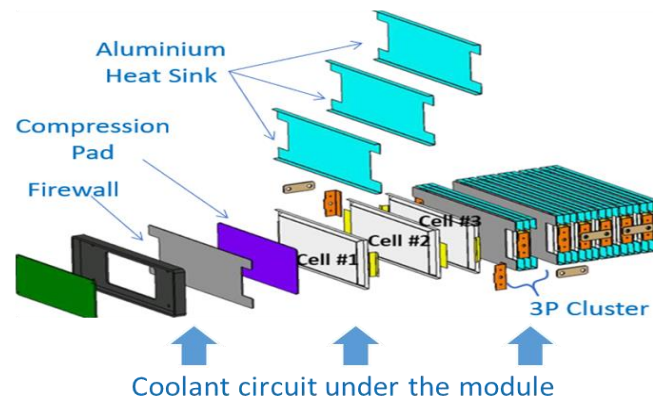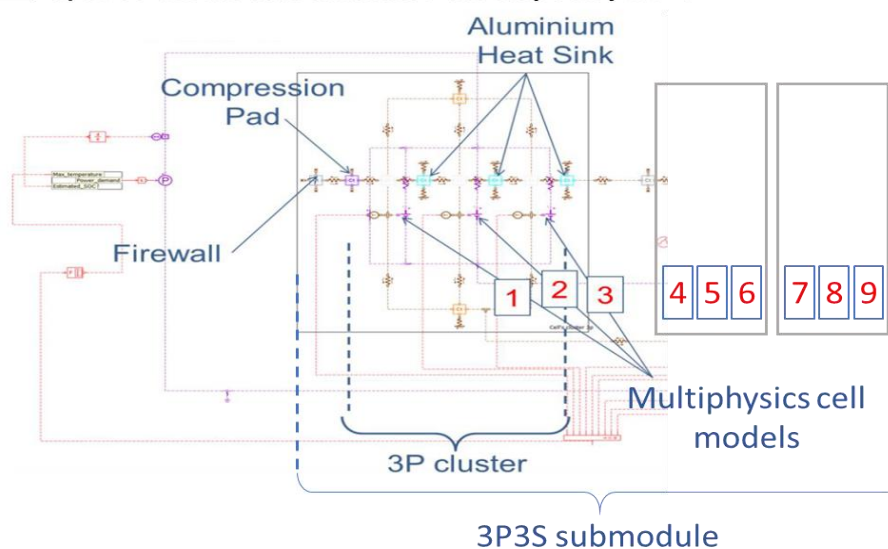

b) 3P3S submodule simulator developed by IFPEN

Figure 13: a) 3P7S module structure proposed by I-FEVS for the vehicle battery pack b) IFPEN 1D thermal runaway propagation model developed on Simcenter Amesim™ software

To obtain the parameters for the 1D propagation model, several experimental campaigns have been carried out:

First the cell thermal runaway model has been developed and calibrated [25] using dedicated Heat Wait and Search (HWS) technique pertaining to Accelerating Rate Calorimetry (ARC) tests performed by Ineris. This cell model is able to account for thermal, electrical behaviours as well as gas release during venting.

Then thermal parameters of the module have been evaluated thanks to IFPEN test bench tests in non-accidental conditions: The thermal response of the module was analyzed through different conditions: with/without electrical solicitation, cooling system On/Off. Based on the experimental results and taking into account the non-homogeneous heat transfer conditions the different exchange thermal coefficients of each cell within the module were optimized.

485 Finally, the performance of the 1D thermal including thermal runaway performance was successfully
486 validated thanks to Ineris abuse tests. As a consequence, the module simulator is then able to predict
487 both thermal and electrical behaviours of the complete module, as can be seen in Figure 14 and Figure
488 15. These figures show the comparison between experimental and model results during a propagation
489 test where the thermal runaway is initiated in cell 5 and the cooling system is working leading to a heat
490 transfer coefficient of 65 W/m²/K with a water at 20°C.

491

492
493
494
495
496
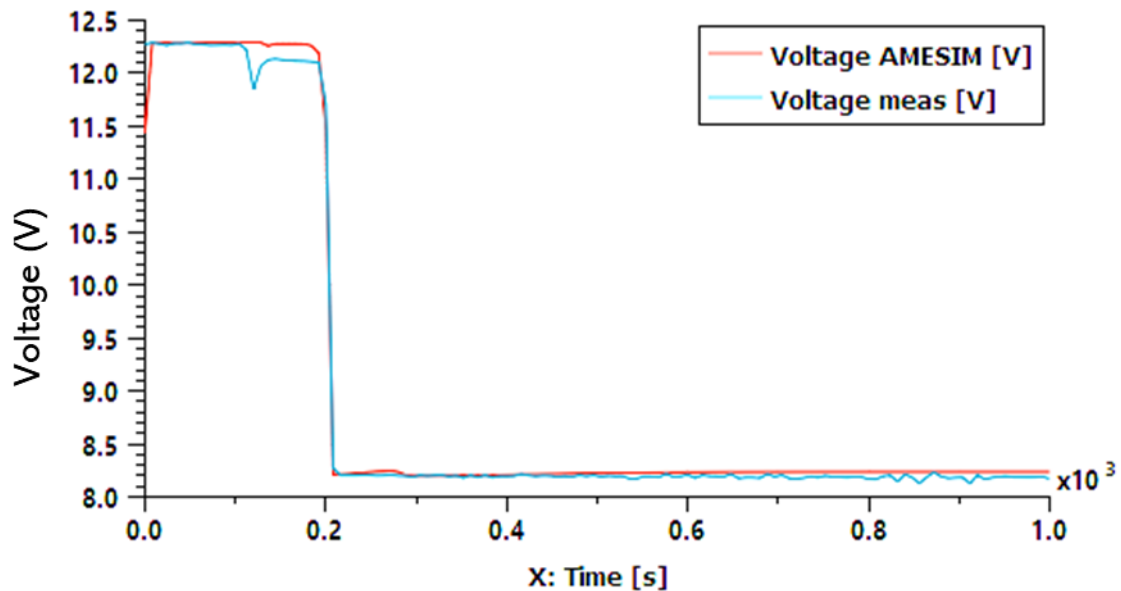
497 **Figure 14: Experimental (meas.) and modelling (AMESIM) results of the electrical evolution**
498 **of the case 4 after a thermal runaway.**
499

500 For each cell, two experimental measurements are available at the top (*meas_up*) and bottom
501 (*meas_down*) of the cell. These experimental results are compared to the numerical results (*AMESIM*).
502 The numerical results are close to the experimental one with a good range of temperature and a good
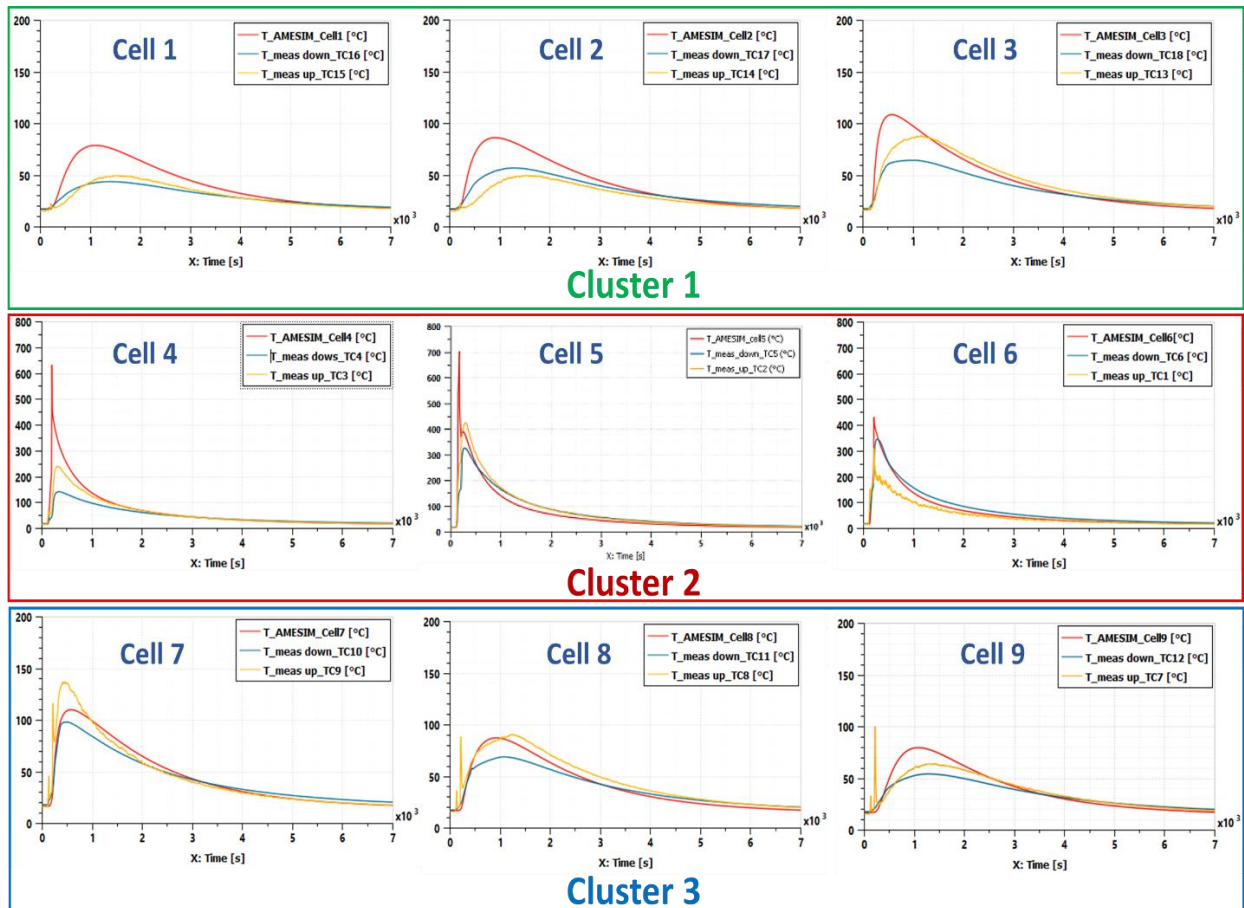503 temporal evolution.

Figure 15: Experimental and modelling results of the cell temperature, case 4.

As a consequence, this model can be further used in a parametric study in order to assess the impact of the firewall thickness on the thermal runaway propagation. The initial firewall is a 1.5 mm thick steel plate. The parametric study evaluated the thermal behavior of the module in cases when the thickness is changed to 1/100, 1/10, 1, 10 and 100 times its initial value. In this simulation the water cooling system is off. The results are shown in Figure 16.

513
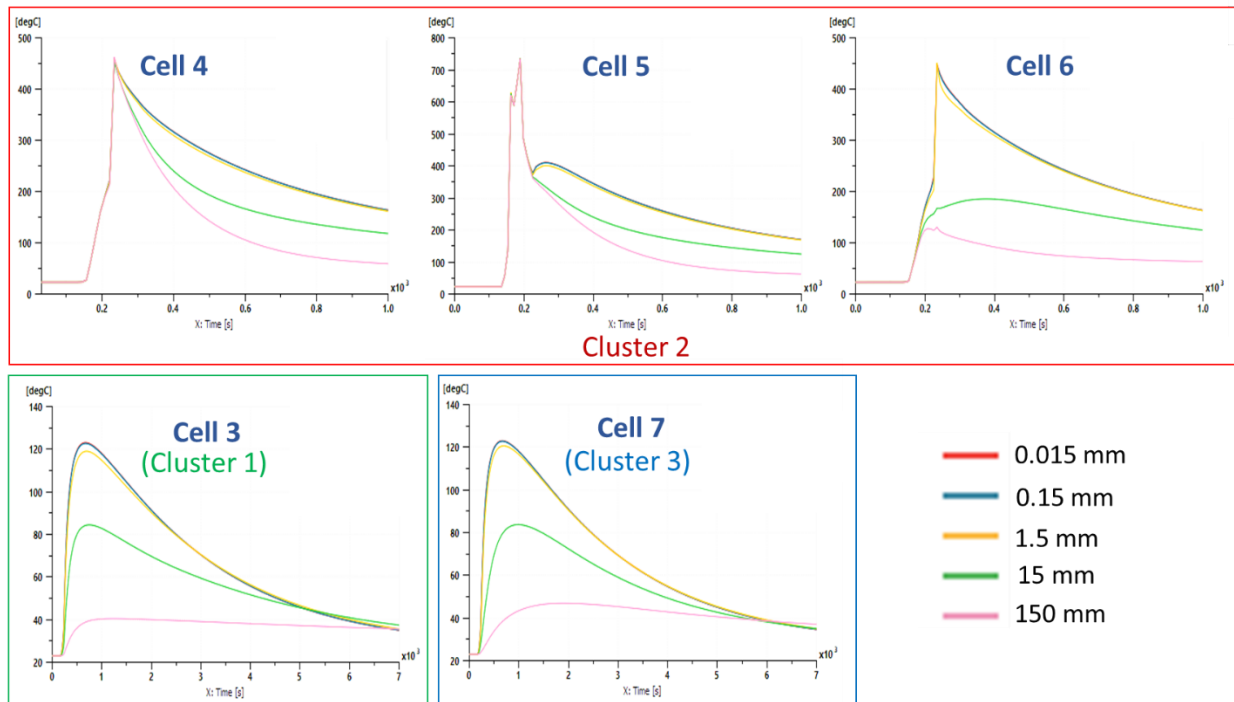
Figure 16: Effect of the firewall thickness on thermal runaway propagation in the central cluster (cell 4, cell 5 and cell 6) and to neighbouring clusters (cell 3 and cell 7).

These results show that no matter the thickness of the firewall, there is no thermal runaway propagation to the neighbouring clusters as cell 3 and 7 do not go into thermal runaway. For higher firewall thickness, thermal runaway propagation may also be prevented inside the central cluster. However this would be achieved at the expense of the overall pack specific energy since the firewalls are weights that are not used for energy storage.

3D thermofluidic model

A detailed 3D thermo-fluidic model has been developed by SAFT (Figure 17), the proposed model targets the thermal behavior of the battery under operating and abuse conditions. The model is built in Simcenter NX, in which the heat transfer module is used to implement the conduction, convection equations while the radiation was ignored. The model considers the heat transfer by conduction in the cells, the pack case, the cooling system, and the air surrounding the cells by convection with a fixed heat transfer coefficient while the air convection in the pack is ignored [25].

According to the computer-aided Design (CAD) of IFEVS, the geometry considered in the model represents an assembly of a single module of a battery module (7S3P = 7 clusters in series with the cluster consists of 3 cells in parallel). The main parameters required are the specific heat capacity, density and thermal conductivity of each solid material, these parameters were given by SAFT and IFEVS.

For the safety analysis, the middle cell (cell 2, group 4) is considered to have the TR. The ARC tests performed by Ineris are used to model the heat flow generated by the thermal runaway of cells. The remaining cells of the module behave according to the heat transfer from a cell in the thermal runaway through different paths (heatsink, busbar, electric contact, etc) (see Figure 17).

540   The abuse model study thermal behavior and the risk of cell-to-cell propagation within the module.
541   No generation of gas by the failure cell is considered in this abuse simulation. The thermal propagation
542   is assumed to be dominated by the thermal conduction of the different paths between the TR cell and
543   the surrounding cells through the electrical contact and the busbar, the contact surface between the
544   cell pocket and the heat sink of the other cells. As gas venting is not considered in this study, the heat
545   transfer by convection and the heat generated by the combustion of the gas cannot be directly taken
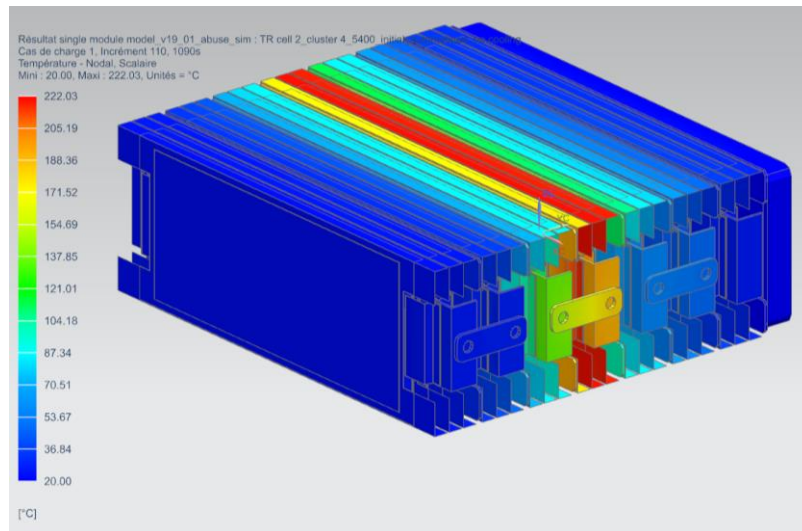546   into account.

547

548   **Figure 17: Thermal runaway propagation from overheat of the middle cell.**
549

550

551   3D CFD model:

552   The thermal behaviour of Li-Ion battery is a complex mechanism where different physics should be
553   considered. Ineris approach consists here to consider each physics with a different way of modelling.
554   First, as shown on previous picture, the chemical process inside the cell is not modelled but considered
555   using the Heat Release Rate (HRR) curve experimentally obtained for each cell. The objective in the
556   future would be to enable the user to evaluate the global battery HRR using a cell scale test. Such an
557   approach opens the possibility to model the effect of the triggering abuse condition on the thermal
558   runaway event.

559   This HRR then enables considering the thermal runaway propagation taking account of both
560   conduction due to the solid contact between the elements and the energy release by the combustion
561   of the electrolyte.

562   The combustion model is based on the FireFOAM CFD code and is used to predict gas dispersion in the
563   surrounding volume, taking into account typically, the quantity of oxygen that can be used due to the
564   battery casing. The model is based on the Navier Stokes equation for fluid flow, coupled with a
565   combustion model to take into account the energy release. The combustion model is then
566   parametrised to correspond the real characteristics of the fuel, here the battery electrolyte. The results
567   of this approach is the temperature distribution in the gaseous phase and radiation from the flame.
568   Those two quantities are then used, also in the code, to estimate the net heat flux on the different
569   surfaces. Such a thermal flux is used as a boundary conditions in the thermal conduction model to
570   predict the inner cell temperature. An example of result is plotted in Figure 18.
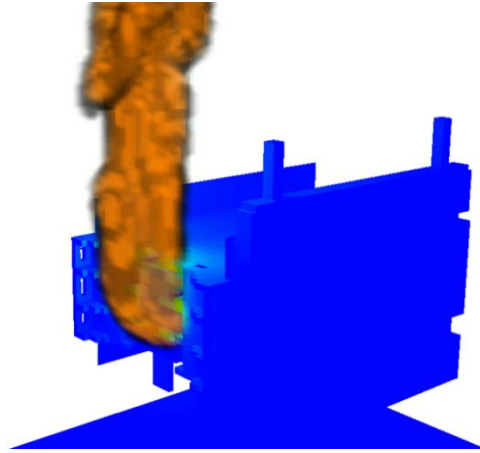
571

572

573

574

Figure 18: Illustration of the 3D CFD model at the cluster level.

576

577 The conduction inside the element is then the key part of the modelling approach. Based on the heat
578 equation, this model takes account for both the energy release by the cell during the first phases of
579 the thermal runaway process, before the cell opens, but also the thermal heat flux coming from the
580 gaseous part due to the electrolyte combustion of the different cells. Obviously, such a model
581 considers the different safety systems that can be introduced inside the battery as insulation plates for
582 example.

583 This approach provides the temperature distribution in the different parts of the battery, typically, this
584 enables the prediction of the temperature rise, due to external heating for each cell. Then, when a
585 given cell reaches the threshold value, typically 120°C, the thermal runaway process is activated in this
586 cell and leads, some seconds after, to electrolyte release and associated combustion.

587 This approach is complementary with those presented previously. It does not predict with high
588 precision the cell behaviour itself as others but consider the influence of the different heating
589 mechanisms.

590

591 Experimental validation: fire contribution

592 To validate the different simulations, a test at module level has been conducted.

593 To initiate the thermal runaway, an internal short-circuit has been induced. The way to trigger the
594 thermal runaway is described in Figure 19. The module is composed of an assembly of 3 clusters, each
595 of them composed of 3 $LiNi_{1/3}Mn_{1/3}Co_{1/3}O_2$ (NMC 111)/graphite flat pouch cells. Each cell has a nominal
596 energy of 70 Wh, a specific energy of 145 Wh/kg measure 220x177x10 mm and were assembled by
597 SAFT (Bordeaux-France).

598 In agreement with the previously presented models, it shows that in case of internal short circuit of a
599 cell, the thermal runaway of the abuse cell is limited to the neighbouring cells and does not affect other
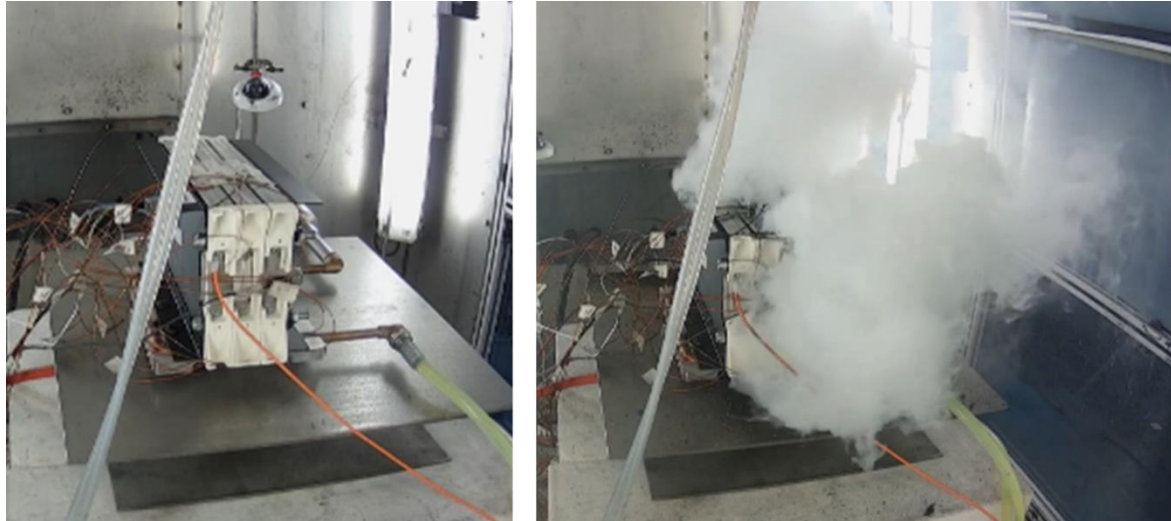600 clusters.

Figure 19: Video extracts of an internal short circuit test of a 3 cluster module.

1.5. Battery Recycling Based on cell BOM

Favoring fast innovation integration in battery technology also requires thinking of End-of-Life (EoL) of previous generation systems. During DEMOBASE project, Accurec has investigated different industrial-scale recycling technologies for lithium ion batteries in Europe. The current recycling industry shows mainly 4 different recycling processes which are shown in Figure 20. Accurec has investigated the elementary recovery rate in individual step in each recycling process for each valuable material.
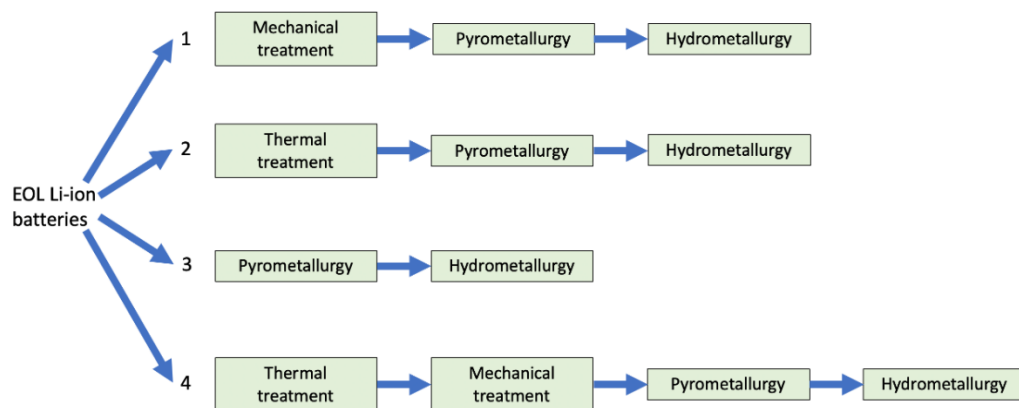

Figure 20: Possible recycling processes for EoL lithium-ion batteries.

The result was collected and integrated into a smart calculation tool which provide recycling yield based on input material of the battery pack and selected recycling process. As a result, the recycling process of battery pack can be theoretically calculated based on cell BOM (Bill Of Materials). 3 different cells, which were developed by SAFT during DEMOBASE project, can be selected as input material (Figure 21), the module (Figure 13) and pack BOM are provided by IFEVS, completing BOM of the whole battery pack.

Figure 21: Input material for calculation tool, from cell to module to pack.

One of the 4 different recycling processes schematized in Figure 20 can be selected by the user in the following window shown in Figure 22 in order to simulate the recycling process. After that, a summary of the selected recycling process is shown in Figure 23.
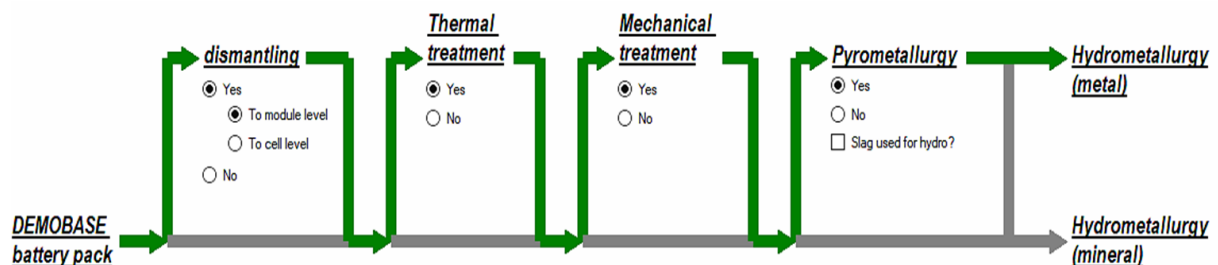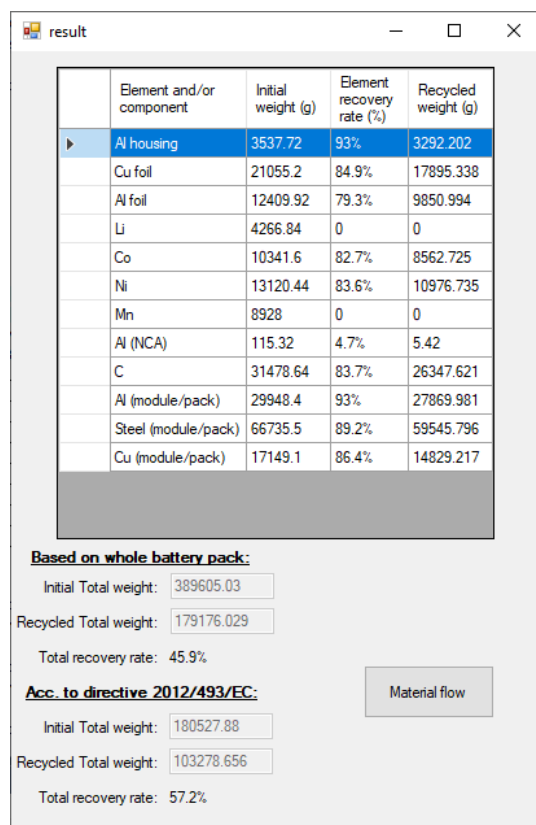

Figure 22: Smart calculation tool process selection window.

As an output of the calculation tool, possible recycling element with its initial input weight, overall recovery rate and recycled weight are listed in a table. Here, all the elements and/or components which could be potentially recycled are listed. The initial weight represents the input weight from the EoL battery pack for the recycling process. The recycled weight represents the weight of output products after the recycling process. Element recovery rate is the product weight divided by initial weight.

A more detailed material flow can be potentially presented (Figure 24) which shows how the selected material flows over each individual step of the recycling process. E.g. for cobalt, the input weight is 10233.72g, no cobalt is lost or recycled by dismantling activity, there is 0.9 wt.% cobalt loss in thermal treatment. Hereafter, it was estimated that 11.8 wt.% cobalt was lost in mechanical treatment resulting in 87.1 wt.% collected for pyrometallurgy process which has another 3.4 wt.% loss. In the end, 83.6 wt.% cobalt was delivered to hydrometallurgy process for deep recovery, separation and refining and 82.7 wt.% is eventually recycled. The most significant cobalt loss appears to take place at mechanical treatment. The calculation tool helps users to understand the recycling efficiency step by step along the recycling process and potentially allows further process improvements.

Element and/or component	Initial weight (g)	Element recovery rate (%)	Recycled weight (g)
Al housing	3537.72	93%	3292.202
Cu foil	21055.2	84.9%	17895.338
Al foil	12409.92	79.3%	9850.994
Li	4266.84	0	0
Co	10341.6	82.7%	8562.725
Ni	13120.44	83.6%	10976.735
Mn	8928	0	0
Al (NCA)	115.32	4.7%	5.42
C	31478.64	83.7%	26347.621
Al (module/pack)	29948.4	93%	27869.981
Steel (module/pack)	66735.5	89.2%	59545.796
Cu (module/pack)	17149.1	86.4%	14829.217

Based on whole battery pack:

Initial Total weight: 389605.03

Recycled Total weight: 179176.029

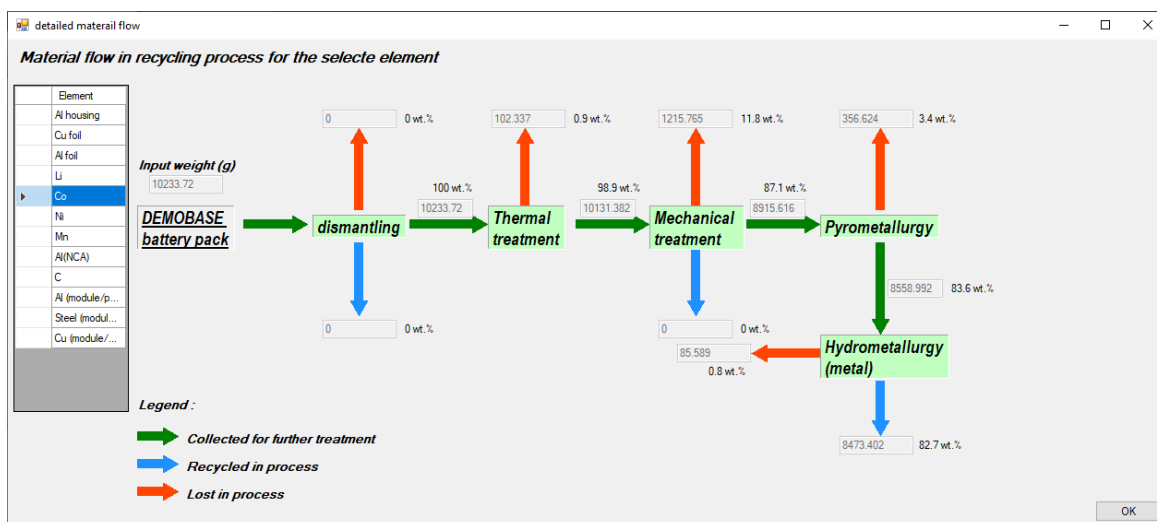Total recovery rate: 45.9%

Acc. to directive 2012/493/EC:

Initial Total weight: 180527.88

Recycled Total weight: 103278.656

Total recovery rate: 57.2%

Material flow

Figure 23: Smart calculation tool result window.

Figure 24: Smart calculation tool detailed material flow window.

641

642 Accurec has investigated different industry scale lithium-ion battery recycling technologies and
643 estimated recycling efficiency of those processes. Based on the battery pack BOM, input material for
644 recycling process can be defined, and subsequently, the recycling product can be also simulated.

645   1.6. BMS:

646   1.6.1. From electrochemical model to BMS

647

648 The electrochemical model which has been developed during the project is mainly based on the well-
649 known Newman's approach. This kind of model needs numerous parameters. Some parameters are
650 design parameters and other ones are relative to intrinsic active material properties, like solid diffusion
651 coefficient in active material, exchange current density, electronic conductivity of the electrode.
652 Indeed, , an important part of the model development activity was linked to the characterization of all
653 these parameters, specific of each active material. The model has been implemented in COMSOL©
654 software and validated against experimental test. Eventually this Full Order Model has been reduced
655 to a single particle model for purpose of BMS integration. For State-of-Charge (SOC) evaluation, a
656 nonlinear observer was used, based on a reduced form of the electrochemical model. More details on
657 the nonlinear observer are given in the article of P.Blondel *et al.[27]*. The layout of applied modeling
658 process is depicted in Figure 25.

659

660 **Figure 25: New framework validated within the project.**

661

662 Final achievement , thanks to the DEMOBASE project, was the validation of this new framework and
663 the identification of several ways of improvement for future research in order to further increase the

664   obtained accuracy. Figure 26 shows on a dynamic electrical vehicle profile the SOC obtained with the
665   observer as compared to real SOC from a perfect current counter on a 17Ah pouch cell.

666   The estimation of SOC is computed for each electrode according to following equation

667

668   $$SOC_{pos} = 100 \times \frac{\left(c_0^{pos} - c^{pos}\right)}{\left(c_0^{pos} - c_{100}^{pos}\right)}$$

669

670   $$SOC_{neg} = 100 \times \frac{\left(c^{neg} - c_0^{neg}\right)}{\left(c_{100}^{neg} - c_0^{neg}\right)}$$

671   where C_{100} and C_0, are the concentrations in Lithium at respectively 100% of SOC and 0% of SOC for
672   the considered electrode (positive (pos) or negative (neg)).

673   and where c^s represents the average concentration of lithium in the electrode s for an average SOC
674   estimation or the surface concentration for an instantaneous SOC estimation

675   Also worth to notice is that the observer enables to estimate instantaneous SOC based on the
676   estimation of the concentration at the surface of the particle which can be valued for vehicle
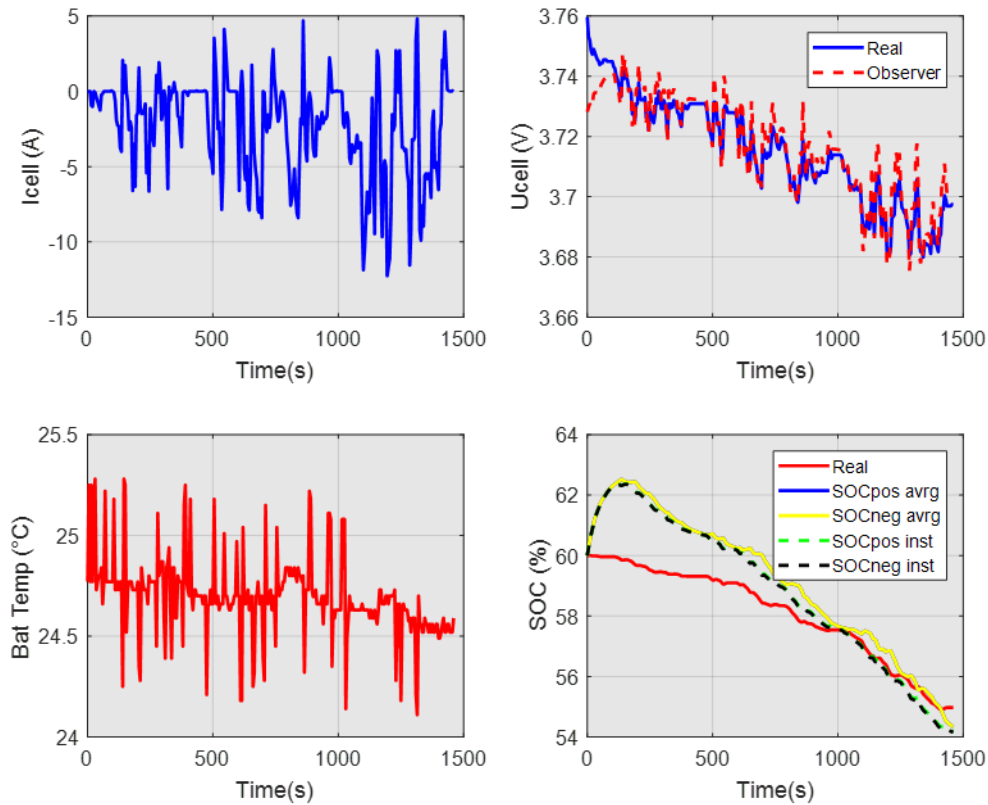677   management.

678

679   **Figure 26: Comparison of SOC from observer and real SOC on dynamic VE profile.**
680

681   The reduced form of the electrochemical model has been also used by a partner of DEMOBASE project
682   to train Neural Network based solution for SOC (see §1.6.2). Finally the evaluation of key performance

683 indicators (KPI) for the project compared this framework to safe operating area (SOA) which is based
684 on equivalent circuit models.

685

686 <u>1.6.2. Advanced solution for SOC assessment</u>

687

688 Most current solutions to determine the State-of-Charge (SOC) are based on high precision current
689 sensors in order to be able to use current integration, better known as Coulomb Counting. However,
690 this method accumulates integration errors over time, which yields in the need for periodic
691 recalibration. This can be done by fully charging the battery to set the SOC at 100%, but the battery
692 might not always be fully charged during a charging step. In this case the battery is not fully charged,
693 a certain rest time is needed before the recalibration, which collides with the intended use of most
694 battery applications. To overcome these issues, many models have been developed, like heuristic
695 models, equivalent circuit models and physics-based models [28]. Additionally, filters like Kalman-
696 filters are applied to the simulation output to get more precise results. Equivalent circuit models are
697 empirical models that do not work well outside of their calibration domain, which limits their use cases.
698 The physics-based electro-thermal models do not suffer from this problem, as they model the real
699 physical behaviour that happens in the battery. Physical models are calibration intensive, because the
700 structure (e.g., electrode geometry) and chemistry (e.g., compounds, mixing rations) of the battery cell
701 must be well known. These parameters are typically trade secrets of the manufacturers and measuring
702 them is time consuming and complex. Additionally, these models tend to be computationally intensive.

703 In addition, all these solutions and models have in common that they require the initial SOC to be
704 known, which is equivalent to the recalibration issue exposed above.

705 A novel approach is to use neural networks to estimate battery state parameters. For the SOC
706 determination, this approach has the benefit that the initial SOC does not need to be known and the
707 need for recalibration is removed. The drawback of neural networks is that many measurement data
708 is needed in order to train the used network. In DEMOBASE, a new approach to overcome this
709 drawback was investigated. A physical battery model was calibrated, as the structure and chemistry of
710 the cell used in the project was known. This physical model was then used to run arbitrary input vectors
711 and generated enough data to train a neural network. The number of measurements needed to
712 calibrate the physical model was much lower than the very extensive and long measurement series
713 that would have been needed to generate the training data for the neural network.

714 Figure 27 shows a neural network-driven simulation output compared to the measured SOC. The
715 simulation methodology was described in [29] The measured SOC was derived from a high-precision
716 current sensor with a calibrated SOC at the beginning of the experiment. The experiment, a real world
717 driving cycle by battery electric vehicle, started with a one hour long constant current draw (light and
718 air condition turned on, no driving), a moderate dynamic driving cycle, followed by a fast charging cycle
719 (50 kW) and again followed by a moderate dynamic driving cycle.

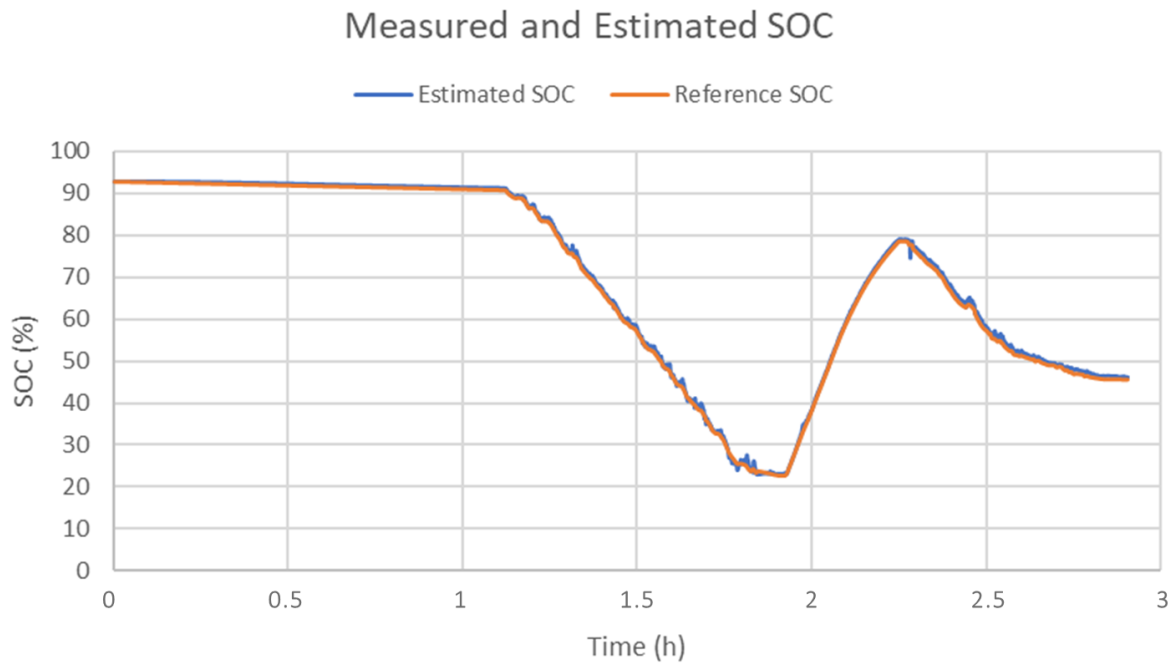## Measured and Estimated SOC

Figure 27: Neural network driven battery cell SOC estimation.

In addition to remove the need for SOC initialization and periodic recalibration, another benefit is that a complex electrochemical model is not needed to be implemented on the BMS anymore, instead only the simple neural network needs to be transferred to the BMS platform. This step is much simpler as neural networks computations correspond to matrix operations, which can be easily implemented and have the additional advantage to be very fast and computational effective.

1.6.3. Advanced solution for safety software (SW) functions

Abuse events in Lithium-ion battery packs are difficult to track at early stages by conventional fault-diagnosis methods. Due to several causes of scattering between cells, even a major abuse event can be considered as a weak signal to track. Open-circuits imply the over-aging of the battery pack and this unexpected loss of power and energy directly impacts the battery availability.

Recent developments in Artificial Intelligence offer new opportunities for weak signals tracking. However, Deep-Learning concepts always require a huge amount of data to be trained, which is nearly unfeasible or time and cost consuming in industrial applications such as battery pack, especially for abuse events testing. To solve this issue, a modelling approach based on a purpose-built equivalent circuit electrical model is used to create and train a neural network for open-circuit fault diagnosis. By combining the architecture of a classification neural network with input data which integrates both measurements and their derivative, the proposed diagnosis method can easily classify data evolving through time and detect an open-circuit in real-time. Indeed, the developed network combines temporality complexity with pattern recognition simplicity.

The methodology is first applied to a battery mock-up with 2P2S-2P battery architecture to allow experimental validation. 183750 patterns are generated by simulation. Then, the same methodology is applied on a full Electric Vehicle battery pack. More than 21 million of patterns are generated by simulation. Generated data correspond to several levels of current, initial state-of-charge, scattering

748 in aging and unbalance. Figure 28 presents the fault diagnosis results obtained experimentally on
749 battery mock-up and Figure 29 presents the fault diagnosis results obtained by simulation on an
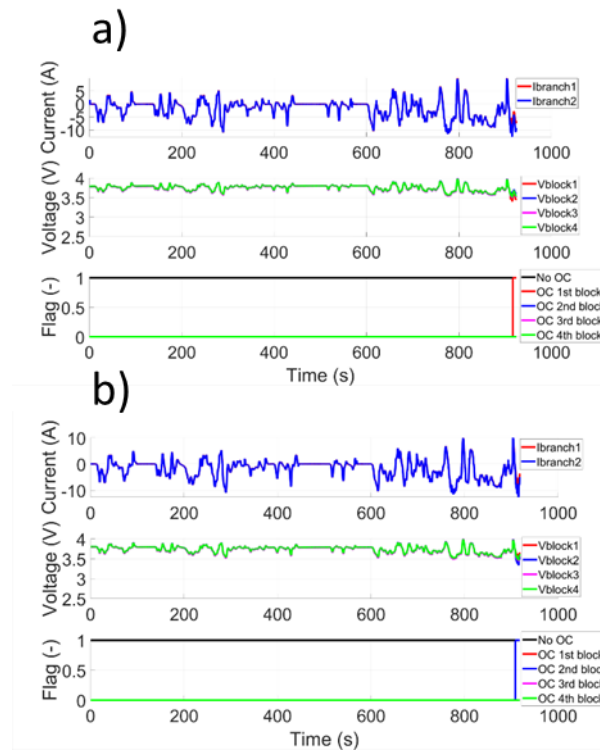750 Electric Vehicle battery pack profile.

751
752

Figure 28: Experimental validation of the fault diagnosis with open-circuit introduced on first block 2P (a) and second block 2P (b).
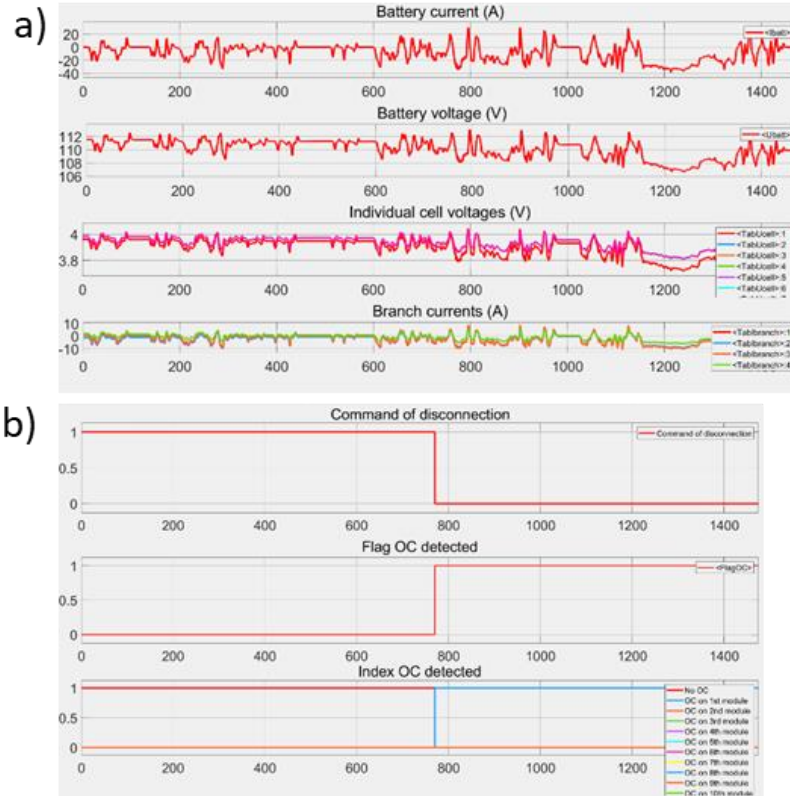
753
754
755

Figure 29: (a) Current and voltage measurements provided to the network. (b) Command of disconnection and results of the fault diagnosis on an Electric Vehicle battery pack model with open-circuit introduced on first module.

The results obtained on an Electric Vehicle battery pack profile validate the reliability of the method. Use modelling to train Neural Networks for the detection of abuse events offers new possible functionalities for safety purpose or maintenance anticipation. Only few tests are required for the validation of the network. It allows keeping physical understanding and knowledges with main effort on modelling to be representative from field.

2. Hardware counter parts design and prototypes

2.1. High energy SiOx cells

BEV vehicle performance is closely linked to lithium-ion cell performances in terms of specific energy, safety behaviour, recyclability, aging. Cell chemistry becomes wide with fast introduction of new active materials. Positive active material can be differentiated by the crystallographic structures: Olivine (eg.: Lithium Iron Phosphate -$LiFePO_4$), lamellar (eg. NCA, NMC), spinel (eg.: $LiMn_2O_4$). Negative electrode for energy cells is mainly based on graphite, amorphous carbon, Silicon, Silicon oxide. To optimize battery performances, blend and composite of several materials are developed. An overview of electrochemical performance of active materials are given in the Figure 30.

With more than 2 times the graphite capacity, SiOx material is an intermediate between graphite and silicon compounds (Si-C). Contrary to high silicon-based materials, SiOx added in few percentages in blend with graphite, limits the lithium consumption during passivation and induces a manageable electrode expansion in charge. Consequently, SiOx-based anodes have similar binders to the classically

781 ones used for graphite. For these different reasons, maturity of this technology is higher than Si-C or
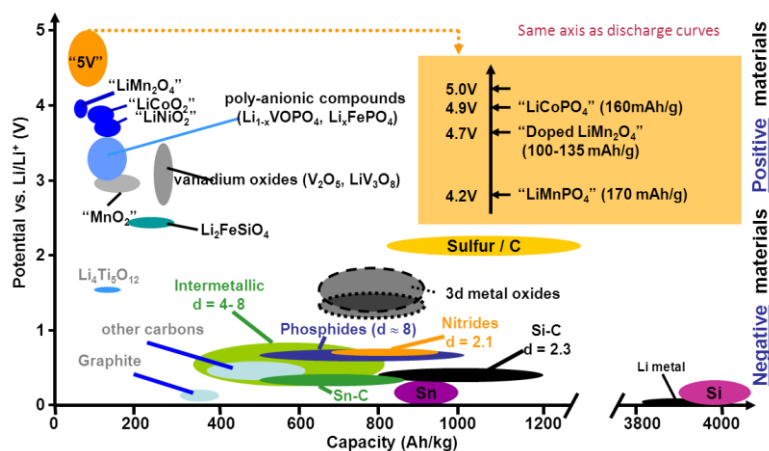782 pure Silicon ones, even though the energy density increase is limited.
783

785 **Figure 30: Lithium-ion Active material overview.**

787 Use of a given recipe is application dependant. It can also be related to raw material cost, which is a
788 driver today for the development of low Cobalt content material like NMC811.

789 Prototyping of pouch cells allow early test of new cell definition from processability to performances.
790 The pictures on the Figure 31 present lab scale active mass ink preparation at Saft before its coating
791 on electrode.

792

794 **Figure 31: Lab scale preparation of electrode ink.**

796 Several prototyped pouch cells have been developed with different designs and capacities. Depending
797 of the application, the performances target and the energy density to reach, the formulation and the
798 design of the electrodes must be specific.

799 In this way, the NMC622 or NMC811 will allow to increase the specific capacity while the definition of
800 the graphite or graphite-SiOx blend impact battery specific capacity. Cell design (electrode thickness,
801 porosity, …) optimizes cell performances on energy, power and lifetime to fulfil battery pack
802 performance specification of range, charging time and lifetime. In this study, a negative electrode active
803 material mixture including up to 15% SiOx has been chosen and the impact on cell performance and
804 safety behavior is examined.
805 A wide range of pouch cells are manufactured from 5 Ah to more than 100 Ah on Saft prototyping
806 lines. They have been used to develop DEMOBASE cells. The Figure 32 presents the pouch cells
807 developed.

808
809

Figure 32: 3 generations of cells for DEMOBASE project with opposite (LS, LU and MU types) tabs and "rabbit type" tabs configuration (Mter type).

812

813 C-rate results are represented in the Figure 33 with NCM811/graphite design in terms of capacity,
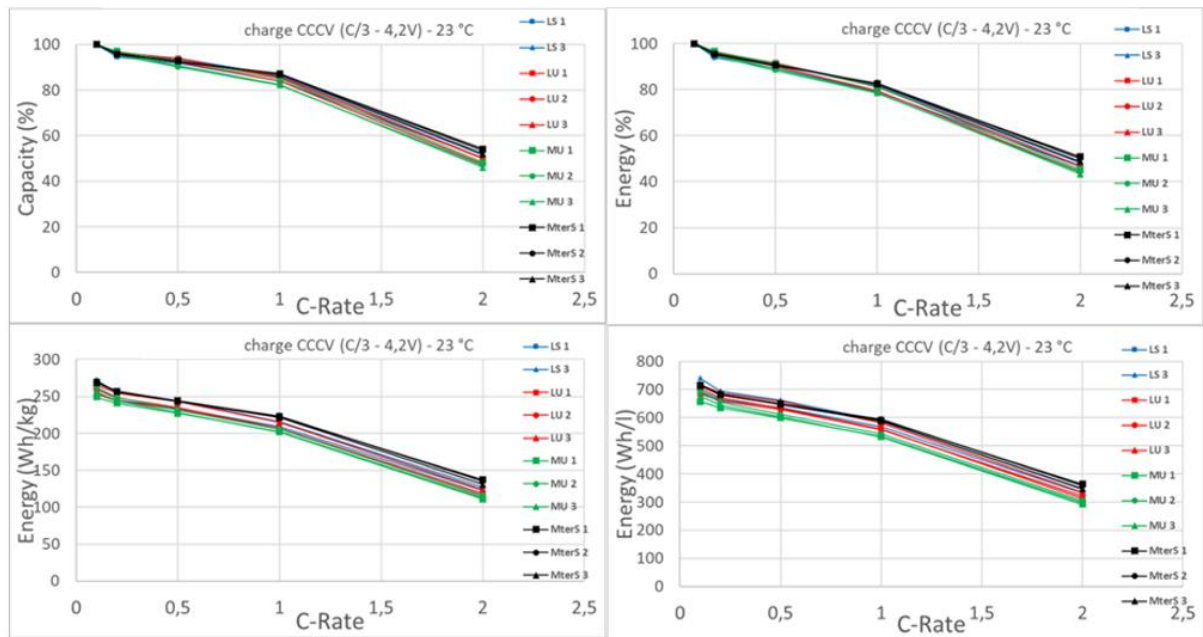814 Energy and specific Energy.

Figure 33: C-Rate for different pouch generations (from LS to Mter type) I. Charge CCCV (C/3-4.2V) – 23 °C.

The specific energy in pouch cells is higher than 250 Wh/kg for the project cells with the highest energy density (Mter pouch cell design). The same design, with NCM811/graphite, in prismatic PHEV2 like cells allows to reach 240 Wh/kg.

2.2. BMS Hardware: Fox BMS

In order to guarantee a safe and efficient operation of the battery system, a battery management system (BMS) is required. The main objective of the BMS is the protection of the battery system from unsafe system states by keeping the battery within its safe operating area (SOA). The second objective of the BMS is the optimum use of the battery system in terms of available power, charge and discharge capacity and lifetime. In practice, these two objectives are not always compatible. For instance, a conservative SOA will ensure safe operation and long battery lifetime. On the other hand, these safety margins will reduce the battery performance, i.e., the available power and useable capacity [30].

In order to overcome this contradiction, the BMS has to provide reliable and highly accurate state estimations, allowing safe operation of the battery without rigid safety margins. This can be reached by a BMS design that provides highest levels of reliability in combination with sufficient computing power to run the advanced sate estimation algorithms as described in this paper. This challenge is addressed in the design of the advanced open source BMS development platform foxBMS. In the course of DEMOBASE, the hardware and software of foxBMS were further adapted, modified and enhanced to fit the requirements of the demonstrator vehicle in the project.

The hardware design files and the bill of materials for foxBMS are available free-of-charge along with the embedded software source code, the software toolchain and the documentation on www.foxbms.org.

843

The basic architecture of foxBMS is designed similar to automotive state-of-the-art systems: BMS Slave Units for measuring cell voltages and temperatures are mounted on each battery module. The BMS Slave Units are then connected to a central BMS Master Unit via a proprietary communication interface depending on the used analog frontend. The software implementing the BMS functionality runs on the microcontroller of the Master Unit. The following list gives a short overview of the functions the BMS Master Unit of foxBMS incorporates:

- Data acquisition from battery sensors: BMS Slave Unit (e.g., individual battery cell voltages and temperatures), global pack voltage sensor (high voltage) and pack current sensor
- Sensor data processing and monitoring of the Safe Operating Area (SOA) of the battery
- State estimation of the battery (e.g., state of charge, state of health, state of function, state of safety)
- Communication with higher level control units (e.g., Vehicle Control Unit)
- Control of actuators (e.g., contactors, chargers, cooling) and additional safety components

In addition, various communication interfaces and memory components (e.g., large non-volatile data storage) are added, meant to be used especially during BMS and algorithm development to support short design cycles. These components, however, may not be part of an industrialized automotive BMS solution for cost reasons. Further, a flexible selection of monitoring solutions provided by various battery monitoring IC manufacturers can be covered using another aspect of the modular approach: the interface electronics between the microcontroller on the Master Unit and the proprietary communication interface of the IC on the slave unit is kept separately as an add-on board. Complementary, the embedded software interface is kept lean to enable easy selection and integration of one of the many supported monitoring solutions.

2.3. Battery pack

The basic criteria adopted can be summarized in the following:

- Develop battery assembly approaches easy adaptable to the continuous evolution of battery cells.

- The in-the-vehicle integration addressing long-term structural robustness-safety including thermal insulation is likely the most competitive and cost-effective route to be addressed. This requires a close collaboration amongst auto manufacturers, Tier1s, semiconductor companies, designer of automated processes for cells and complete battery packs. The purpose being the development of standardized cost competitive and high performing energy storage solutions easily adaptable to the requirements of the majority of Original Equipment Manufacturers (OEMs).

- Reduced safety over time (aging) due to time increasing electro-thermal expansion and retraction of battery cells. For instance, pouched cells during charging and discharging tends to expand in and re-tract thickness some 1% up to 8% when electrodes have a high content of silicon. Aged pouched cell even when using electrodes with low content of silicon might increase their thickness some 8% when at their 80% of the initial capacity [31].

- The safe integration of cells into modules then into battery packs poses heavy electro-mechanical constraints. Cylindrical cells are less critical than pouched cells because they are not packed in close contact, but the problem remains critical also for cylindrical cells.

886   •   Limited modularity and high cost battery pack assembly on top of the cost of battery cells.
887   Many approaches are currently explored to address modular battery systems adaptable to
888   different vehicle architecture. The battery pack optimisation in the context of vehicle
889   integration cost reduction considering passenger ergonomics, structural safety and thermal
890   insulation remains a far less than a mature topic.

891

892   2.4. Battery disconnect switch: Design and demonstrator
893 One of the probably most critical functions of battery management is the battery disconnect switch,
894 which separates the high voltage / high energy / high power battery from the rest of the car's electrical
895 net. Up to now, rather bulky and heavy mechanical switches are featured to cut off the current flow
896 as quickly and as complete as possible in case of emergencies. Semiconductor switches can do that job
897 by >3 orders of magnitude faster with much less than half the weight and volume. Figure 34 shows the
898 basic electrical circuitry to employ them.

899

900
901
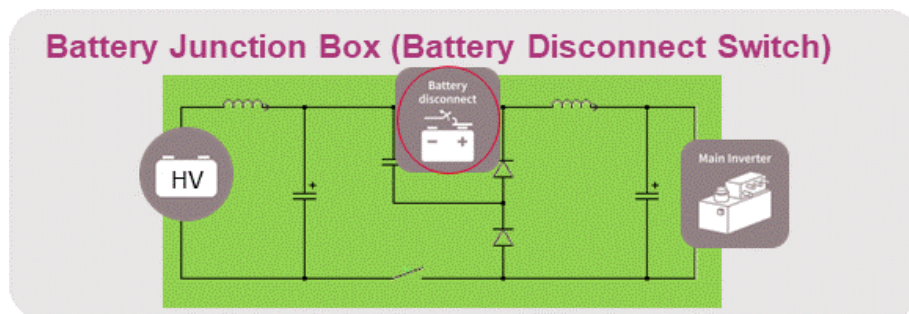
902   **Figure 34: Basic circuitry for a semiconductor-based battery disconnect switch.**
903
904

905 The optimisation of the transistor characteristics and its cooling protocol within an optimised
906 package has been one of the goals in DEMOBASE. The voltage and current traces of the
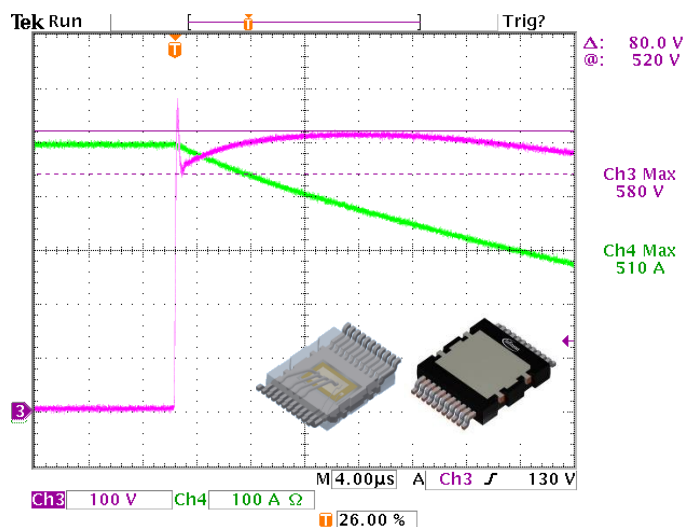907 demonstrator shown in Figure 35 demonstrate a significant step towards this goal.

908

909   **Figure 35: A semiconductor-based battery disconnect switch safely shuts off 500A at a**
910   **nominal voltage of 450V.**

911
912 In this short circuit turn-off test on a demonstrator consisting of five 10mOhm 600V MOSFETs, a
913 current of about ~ 100A per device at Vin=450V could be switched off within microseconds without
914 destruction.
915 Providing devices optimized for critical BMS-functions, enables new opportunities in functionality,
916 versatility, and enhanced intrinsic safety for battery system developers.

917

918 2.5. Cell pressure sensor: Design and demonstrator

919

920 A second device further developed in DEMOBASE is a sensor to measure directly the pressure inside a
921 battery cell. Figure 36 shows on the left the basic concept as a schematic cross-section of a sensor
922 glued directly over a hole in the wall of a battery cell, and on the right a modified automotive pressure
923 sensor, which has been employed for this setup.

924

925

926
927
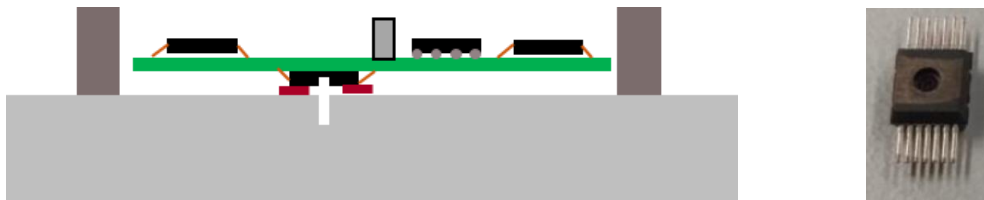
Figure 36: Basic concept (left) of a sensor (right) to monitor the pressure inside a battery cell.

930
931

932 Through the pressure port, a set of capacitive membranes and suspension elements are exposed to
933 the medium, of which the pressure is to be measured. Since the electrolyte of battery cells in almost
934 all cases contains rather aggressive components, it is advisable to cover the exposed parts of the
935 pressure sensor with an inert material, which - of course - must not deteriorate the functionality of the
936 sensor membrane.

937 Besides testing the durability of different gel options, the impact of such a gel plug on the sensor
938 functionality has been a focus of the DEMOBASE development. Figure 37 shows, as one of the results,
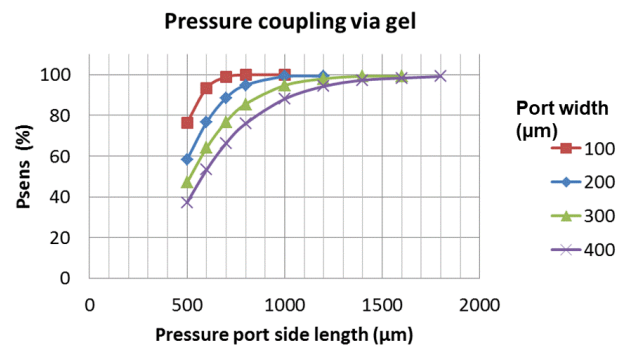939 the reduction in the pressure reading as a function of different pressure port sizes.

940

Figure 37: Reduction in the pressure reading by different pressure port sizes.

941

942 Evidence has been shown that an increase in cell pressure over cycling, is non-linear phenomenon with
943 temperature. Besides the additional safety margin by early & distinct detection of troubles, this could
944 be used as independent, additional input for (State of Health) SoH calculations [32].

945 <u>3. Proposition for a sustainable and low cost investment vehicle</u>
946 <u>3.1. requirements for dismantling</u>
947 Before recycling, the EV battery pack must be dismantled. Due to the large battery capacity and high
948 voltage of a battery pack, the battery pack can be only dismantled by qualified engineers. Accurec has
949 investigated structures of several inhouse battery packs from different electric vehicle OEMs. Based
950 on these investigations, the following dismantling process for electric vehicle battery pack was
951 recommended. The dismantling process steps are:

952 1. Remove the disconnector plug and voltage measurement
953 This should be the first step of dismantling since, removing the disconnector partially disconnects the
954 circuits and reduces the voltage, on the other hand, contacts are available for measuring the voltage
955 of the battery system.

956 2. Open the battery pack housing
957 Depending on the sealing technology, housing parts can be connected by screws or sealing or (laser)
958 welding etc. Nowadays, most housing parts are connected by screws which is relatively easy and safe
959 for dismantling. When housing parts are connected by sealing or welding, special care should be
960 taken during opening the housing regarding safety, since housing parts are strongly connected,
961 resulting in the need of applying cutting tools. Without knowing the internal structure, cutting the
962 pack housing is likely to produce in heat, sparks, vibrations into the battery pack resulting in potential
963 short-circuits of the modules/batteries or other further safety risks.

964 3. Remove the cooling system
965 The cooling system might cover a large area of the battery pack in order to provide cooling
966 performance. In this case, the cooling system has to be removed first. An air-cooling system consists
967 of inserted plastic channels and is usually easy to remove. In the case of a liquid cooling system,
968 attention should be paid to the possibility of liquid leakage resulting in contaminating the rest of the
969 battery pack and inducing further safety risks e.g., battery short-circuit or chemical reaction between
970 chemicals.

971 4. Release the connection between cell and cell controller and remove the electronic circuits
972 Each cell connects to the cell controller separately. Normally, these connections are built together as
973 strands for a battery pack. If the electrical connections to the cell controller are disconnected in a
974 wrong sequence, this can lead to overvoltage in the electronics and destroy them (fire risks).
975 Therefore, the correct disconnection order must be strictly observed. Then all electronic parts e.g.,
976 control board and cell controller, beside battery packs should be removed carefully.

977 5. Release the connection between copper wire and the battery pack
978 The next step is removing wires which connect to cell modules and thereby disconnect the circuit.
979 Exposed ends of wires should be insulated with tape until final removal. Depending on the number of
980 cells per module and on the internal connection modus (in series or parallel), the voltage of cell
981 module varies. Nowadays, the voltage of module is normally lower than 60 Volt which is in- between
982 low and high voltage in Electric Vehicle application based on an UN agreement. Therefore, module
983 can now be made relatively safe for further disassembling.

984 6. Remove modules and further dismantling

985 In this step, all connections between modules to battery pack housing are disconnected. The
986 modules are linked to the battery pack in different ways depending on the attachment technology,
987 resulting in different tools to be used in this step. Regarding safety, special care should be taken
988 when these connections are disconnected during cutting, since these actions are likely to induce
989 battery short-circuit and other safety issues. When the module is removed from the battery pack, the
990 inside-cells can be safely removed from the module, just as normal lithium-ion batteries in consumer
991 electronics.

992 The above-mentioned dismantling process assures the highest dismantling and recycling safety for
993 the DEMOBASE battery pack.

994

995 ### 3.2. Vehicle design and prototype: Low investment manufacturing of vehicles
996 The DEMOBASE vehicle has been developed by applying the Flexible, Agile and Lean manufacturing
997 approach being implemented in the I-FEVS microfactory, the result of common activities among CLN-
998 GROUP MA, IFEVS and Comau driven by the concepts developed in a cluster of EU projects.

999 While most of the debate is on batteries and electric powertrains, the major challenge still facing the
1000 automotive industry is to reduce energy, time and investments (costs) in the manufacturing of
1001 automotive chassis. The investment needed to produce a new safe chassis suitable for an electric
1002 vehicle is usually higher than 100M€, thus making the return of the investment very uncertain. The
1003 construction of moulds, metal sheet stamping and robotic assembly are time and high energy
1004 consuming processes. Furthermore, the conventional manufacturing through metal sheets does not
1005 allow flexibility or agility: once the chassis is made, changes are cost prohibitive.

1006

1007 In an area of only 1500m^2, the flexible and agile manufacturing of the body frame is carried out without
1008 the expensive moulds, stamping and robot assembly usually required by the conventional method of
1009 metal sheet forming, adopted by the OEMs and their chassis suppliers. Besides, thanks to the approach
1010 used to cut the high strength steel tubes by a robotized laser system for the welding of the complete
1011 chassis, there is no need for complex templates. The same area covers the production of doors, axle
1012 systems, suspension arms and wheel hubs.

1013 On the contrary, the current automotive manufacturing technology, shown in Figure 38 is
1014 characterized by:

1015 - Complexity of moulds to stamp metal sheets in a 3D geometry (Figure 38 left)
1016 - Complexity of tooling to assemble/weld the moulded components (Figure 38 right**)**
1017 - Lack of flexibility, e.g., great differences are needed between chassis configurations with
1018 different door numbers
1019 - Large production volumes are necessary for acceptable ROIs.
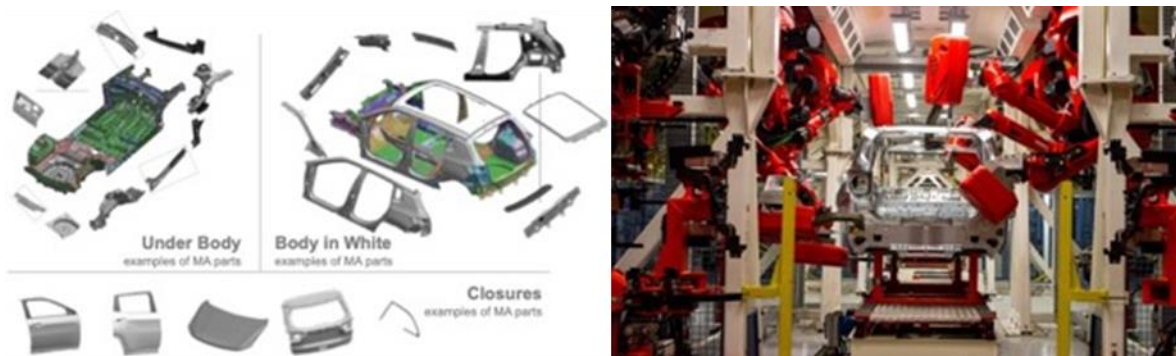1020

Figure 38: Complexity of the current manufacturing process of automotive chassis.

1021 The microfactory is conceived to manufacture 50 vans/day over two shifts and 220 days/year.
1022 Whether the annual production capacity of 11,000 units would not be sufficient to meet the
1023 demand, it could be increased by implementing a third daily shift.

1024 The final DEMOBASE vehicle developed with the criteria explained above is shown in Figure 39.

1025

1026

1027 **Figure 39: DEMOBASE vehicle.**

1028

1029 Conclusion
1030 The activities and key non-confidential results of DEMOBASE EC H2020 GV7 project are presented with
1031 limited details in this publication. It is reminded to the readers that parent papers have been made
1032 available at earlier stage with much more details on some of the aspects discussed more
1033 straightforward here (see SI, also to access more information on the DEMOBASE research organisation
1034 lay-out and recap of main objectives and relating demonstrators). They point out that simulation-
1035 based design of the battery system pack is already a key vector to improve efficiency, by sharply
1036 reducing development time and supporting all phases from early design to safety related activities.
1037 Some Key Performance Indicators are given in the technical results in terms of vehicle efficiency, fail
1038 operational capability of the battery pack, and proposal for low investment cost.
1039
1040 The results draw some strong conclusions:
1041 • Cell management can be developed in hidden time, without any physical part for most of the
1042   activities, from active material characteristics, using cell and battery digital mock-up.

- The battery dismantling strongly depends on its assembly technology: glue, welding, screw; and its BMS communication capability for Authorized treatment Facilities (AFT) to organise battery second life and to safer recycle the battery. The potential end of life additional cost for recycling of BEV is not counterbalance today in initial vehicle cost as it is today for combustion engine car with fuel consumption.
- An unexpected result of sudden increase of battery aging highlights that higher energy density cannot be balanced by decrease of cell robustness, making second-hand market weaker.
- Battery safety is efficiently supported by simulation and tests at low scale level; a challenge is still to consider gas dispersion and its fire risk. Battery safety is improved using advanced devices.

Multi-level modelling and testing from material to manufacturing is still a challenge for the battery industry. Their development and implementation enable lower cost and faster innovation and will be a differentiation item in the industrial competition; DEMOBASE is a contribution to their achievements.

The authors of this paper deeply hope that the DEMOBASE project has constituted a valuable step toward scientific-sound integration of innovation in safe and environmental-friendly development of EVS. Beyond this goal, they also think that data provided may serve further related standardization efforts in the field, as exemplified by BSI PAS 7060[33] and IEC TC21, SC21A and TC120 published documents and projects

CRediT authorship contribution statement

Conducting paper drafting and final editing through settlement of editorial committee: P. Desprez, A. Bordes, D.L. Danilov, A. Lecocq & G. Marlair; Abstracts, Introduction & conclusion: P. Desprez, G. Marlair, & D.L. Danilov;

Operational research activities (by paper sections) as follow: E. Durling & S. Kolari (SW collaborative platform), P. Desprez, A. Dominget, L. Hamelin, S. Herreyre & G. Rigobert (safety test cell with heater design and prototyping), D.L. danilov, Z. Chen, L.H.J. Raijmakers, D. Li, J. Zhou & P.H.L. Notten (cell aging assessment), M. Petit, J. Bernard & J. Martin (EV performances evaluation), P. Perlo, M. Biasiotto, R. Introzzi (Battery pack architecture design and construction), A. Lecocq, A. Bordes, B. Truchot & G. Marlair (gas flammability and emission toxicity), B. Truchot, A. Lecocq, A .Bordes, G. Marlair, M. Petit, J. Bernard, J. Martin & M. Belerrajoul (Thermal runaway propagation testing, modeling and risk management), Z. Wang & C. Siret (battery recycling strategy), S. Benjamin & N. Legrand (BMS design), S. Koffel & V. Lorentz (adanced solution for SOC assessment), S. Laurent & M. Dahmani (advanced solution for safety SW functions), P. Desprez, A. Diminget, L. Hamelin & S. Herreyre (design and prototyping high energy SiOx cells), S.Koffel & V. Lorentz (BMS hardware concept), W. Maurer (Battery safety disconnect switch and cell pressure sensor design and demonstrator), Z. Wang, P. Pierlo, M. Biasotto, R. Introzzi, J. Lamontanara & M. Massazza (sustainable low cost investment vehicle principles and vehicle demonstrator)

Declaration of competing interest

The authors declare that they have no known competing financial interests or personal relationships that could have appeared to influence the work reported in this paper.

Acknowledgments

REFERENCES

[1] X. Sun, Z. Li, X. Wang, C. Li, Technology development of electric vehicles: A review, Energies 13(1) (2020) 90.

[2] https://en.wikipedia.org/wiki/History_of_the_electric_vehicle, (late access Oct. 2020, 6th).

[3] DOE, The history of the electric car, https://www.energy.gov/articles/history-electric-car, late access Oct. 2020, 6th (2014).

[4] https://egvi.eu/wp-content/uploads/2018/01/electrification_roadmap_web.pdf, late accessNov. 2020.

[5] European Battery Alliance web site: https://www.eba250.com/; late access Oct. 2020.

[6] H. Das, M. Rahman, S. Li, C. Tan, Electric vehicles standards, charging infrastructure, and impact on grid integration: A technological review, Renewable and Sustainable Energy Reviews 120 (2020) 109618.

[7] https://pushevs.com/2020/10/26/cobalt-free-lfp-battery-cells-from-guoxuan-to-reach-260-wh-kg-in-2022/ , late acces Nov. 2020.

[8] https://pushevs.com/2020/10/12/ora-is-getting-closer-to-its-goal/, late access Nov. 2020.

[9] https://pushevs.com/2020/09/29/svolt-unveils-interesting-data-on-its-cobalt-free-batteries/, late access Nov. 2020.

[10] Bloomberg, Battery Pack Prices Cited Below $100/kWh for the First Time in 2020, While Market Average Sits at $137/kWh, https://about.bnef.com/blog/battery-pack-prices-cited-below-100-kwh-for-the-first-time-in-2020-while-market-average-sits-at-137-kwh/ late access august 2021 (2020).

[11] https://pushevs.com/2020/08/26/wuling-hong-guang-mini-ev-had-a-strong-first-full-sales-month/ , late access Nov.2020.

[12] https://cleantechnica.com/2020/03/28/check-out-this-electric-vehicle-total-cost-of-ownership-calculator/, late access Nov. 2020.

[13] Tesla's secret batteries aim to rework the math for electric cars and the grid, Reuters Technology news (2020).

[14] https://www.rethinkx.com/news , late access Nov. 2020.

[15] A. Kampker, D. Vallée, A. Schnettler, Elektromobilität, chapter Production von Elecktrofahrzeugen, Springer2013.

[16] https://fmi-standard.org/, late access Nov. 2020.

[17] https://www.modelica.org/modelicalanguage, Late access Nov. 2020.

[18] https://www.nrel.gov/docs/fy17osti/66958.pdf, late access Nov. 2020.

[19] D. Li, Aging mechanisms of Li-ion batteries: seen from an experimental and simulation point of view, (2017).

[20] D. Danilov, R. Niessen, P. Notten, Modeling all-solid-state Li-ion batteries, Journal of the Electrochemical Society 158(3) (2010) A215.

[21] D. Li, D.L. Danilov, L. Gao, Y. Yang, P.H. Notten, Degradation mechanisms of the graphite electrode in C6/LiFePO4 batteries unraveled by a non-destructive approach, Journal of The Electrochemical Society 163(14) (2016) A3016.

[22] D. Li, D. Danilov, Z. Zhang, H. Chen, Y. Yang, P.H. Notten, Modeling the SEI-formation on graphite electrodes in LiFePO4 batteries, Journal of The Electrochemical Society 162(6) (2015) A858.

[23] P. Ribière, S. Grugeon, M. Morcrette, S. Boyanov, S. Laruelle, G. Marlair, Investigation on the fire-induced hazards of Li-ion battery cells by fire calorimetry, Energy & Environmental Science 5(1) (2012) 5271-5280.

[24] S. Abada, G. Marlair, A. Lecocq, M. Petit, V. Sauvant-Moynot, F. Huet, Safety focused modeling of lithium-ion batteries: A review, Journal of Power Sources 306 (2016) 178-192.

[25] X. Feng, L. Lu, M. Ouyang, J. Li, X. He, A 3D thermal runaway propagation model for a large format lithium ion battery module, Energy 115 (2016) 194-208.

[26] S.A. Martin Petit, R. Mingant, J. Bernard, P. Desprez, P. Perlo, M. Biasotto, R. Introzzi, A. Lecocq G. Marlair, DEMOBASE project: Numerical simulation for seamless integration of battery pack in light electric vehicle, 32nd Electric Vehicle Symposium (2019).

1141 [27] P. Blondel, R. Postoyan, S. Raël, S. Benjamin, P. Desprez, Nonlinear circle-criterion observer
1142 design for an electrochemical battery model, IEEE Transactions on Control Systems Technology 27(2)
1143 (2018) 889-897.
1144 [28] R. Zhang, B. Xia, B. Li, L. Cao, Y. Lai, W. Zheng, H. Wang, W. Wang, State of the art of lithium-ion
1145 battery SOC estimation for electrical vehicles, Energies 11(7) (2018) 1820.
1146 [29] S. Bockrath, A. Rosskopf, S. Koffel, S. Waldhör, K. Srivastava, V.R. Lorentz, State of Charge
1147 Estimation using Recurrent Neural Networks with Long Short-Term Memory for Lithium-Ion
1148 Batteries, IECON 2019-45th Annual Conference of the IEEE Industrial Electronics Society, IEEE, 2019,
1149 pp. 2507-2511.
1150 [30] D. Andrea, Battery management systems for large lithium ion battery packs, Artech house2010.
1151 [31] LG data Sheet, (2019).
1152 [32] J. Schmitt, A. Jossen, Influence of State of Charge, Temperature and Aging on the Gas Pressure
1153 inside Prismatic Lithium Ion Cells, (2020).
1154 [33] D. Walker, PAS 7060:2021Electric vehicles – Safe and environmentally-conscious design and use
1155 of batteries – Guide, (2021).

1156

1157